Inorganic Chemistry

Article

pubs.acs.org/IC

Exploiting Framework Flexibility of a Metal−Organic Framework for Selective Adsorption of Styrene over Ethylbenzene

Soumya Mukherjee,[†] Biplab Joarder,[†] Aamod V. Desai,[†] Biplab Manna,[†] Rajamani Krishna,[‡] and Sujit K. Ghosh*[,†]

[†]Indian Institute of Science Education and Research (IISER), Dr. Homi Bhabha Road, Pashan, Pune-411008, India

[‡]Van't Hoff Institute for Molecular Sciences, University of Amsterdam, Science Park 904, 1098 XH Amsterdam, The Netherlands

Supporting Information

ABSTRACT: The separation of styrene and ethylbenzene mixtures is industrially important and is currently performed in highly energy-intensive vacuum distillation columns. The primary objective of our investigation is to offer an energy-efficient alternative for selective adsorption of styrene by a flexible metal−organic framework, DynaMOF-100. The structural transformation of DynaMOF-100 is specifically triggered on inclusion of styrene within the framework; this structural transformation is reversible. The styrene/ethylbenzene adsorption selectivity, originated as an outcome of the framework flexibility, is found to be much superior to the only two MOFs yet reported, serving styrene/ethylbenzene separation purpose.

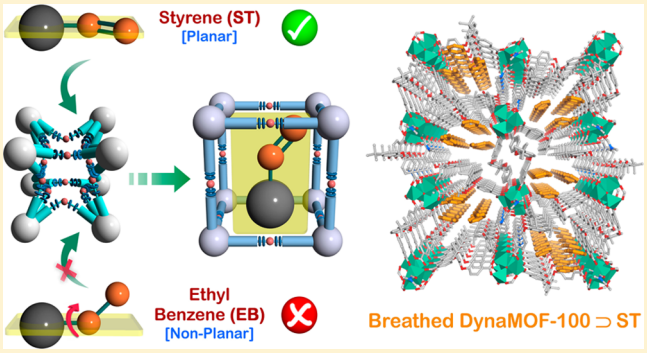

INTRODUCTION

Owing to the high reactivity of its vinyl group, styrene (ST) is an important feedstock in the petrochemical industries.[1] Alkylation of benzene with ethylene produces ethylbenzene (EB), which is dehydrogenated to form ST, a monomer used in the manufacture of many commercial polymers and copolymers. The conversion of EB to ST is only partial, and the reactor product contains a large fraction, in the range of 20%−40%, of unreacted EB.[1,2] Because of the small difference (9 K) in boiling points (ST (bp 418.3 K) and EB (bp 409.3 K)), the separations are currently achieved in vacuum distillation columns, which are energy-intensive. Adsorptive separations using microporous metal−organic frameworks (MOFs) offer energy-efficient alternatives to distillation.[3−12] Several MOFs have been demonstrated to offer substantial potential for use in the separation of xylene isomers,[5,6,13−18] hexane,[19−22] or the C_5 fraction-compounds formed by steam crackers, benzene/cyclohexane separation, and removal of heterocyclic aromatic compounds from fuels.[13,23−27] Flexible MOFs are of particular interest because of their tunable structural flexibility leading to guest-specific breathing phenomena of the pore windows/channels.[26,27] Despite its industrial importance, research on the targeted development of suitable MOFs for ST/EB separations has been rather limited.[28−30] Maes et al.[28] and Remy et al.[29] have demonstrated that MIL-47 (V) and MIL-53 (Al) are of potential use in the separation of mixtures of ST and EB. However, the adsorption selectivities achieved with these two MOFs are rather low and fall in the range of 6−10.

Recently, we reported the synthesis of a dynamic structure-based MOF compound showing clear *p*-xylene (PX) preference over its congener C_8-alkylaromatic isomers at ambient temperatures by framework-breathing and guest-induced reversible solid-state structural transformations.[18,20] The structure of this MOF, hereinafter referred to as DynaMOF-100, gets transformed in such a manner as to allow optimal packing of PX within the cavities. The strong selectivity of DynaMOF-100 for PX was established in our published work,[18] but the separation performance of this material in comparison to the established MOFs and industrially employed zeolites were not included in our earlier work. Therefore, the Supporting Information accompanying this publication provides detailed comparisons of DynaMOF-100, MAF-X8,[31] and BaX zeolite for separaton of *o*-xylene (OX)/*m*-xylene (MX)/*p*-xylene/EB mixtures. The data presented in Supporting Information, including Figures S20−S23 and the video animation-illustration, clearly show that DynaMOF-100 has both significantly higher selectivity and uptake for PX as compared to MAF-X8 and BaX zeolite, making it the best adsorbent material for this separation duty.

In our current investigation, this soft porous crystalline material DynaMOF-100 (compound **1**) was comprehensively investigated for the targeted separation of EB- and ST-containing feed mixture by exploiting the highly dynamic adaptable feature of the framework. As described, herein the compound **1** is the desolvated squeezed two-dimensional (2D) phase (of almost nonporous nature; Figure 1b and Supporting Information, Figure S5) resultant from the porous as-

Received: January 28, 2015
Published: April 15, 2015

DOI: 10.1021/acs.inorgchem.5b00206
Inorg. Chem. 2015, 54, 4403−4408

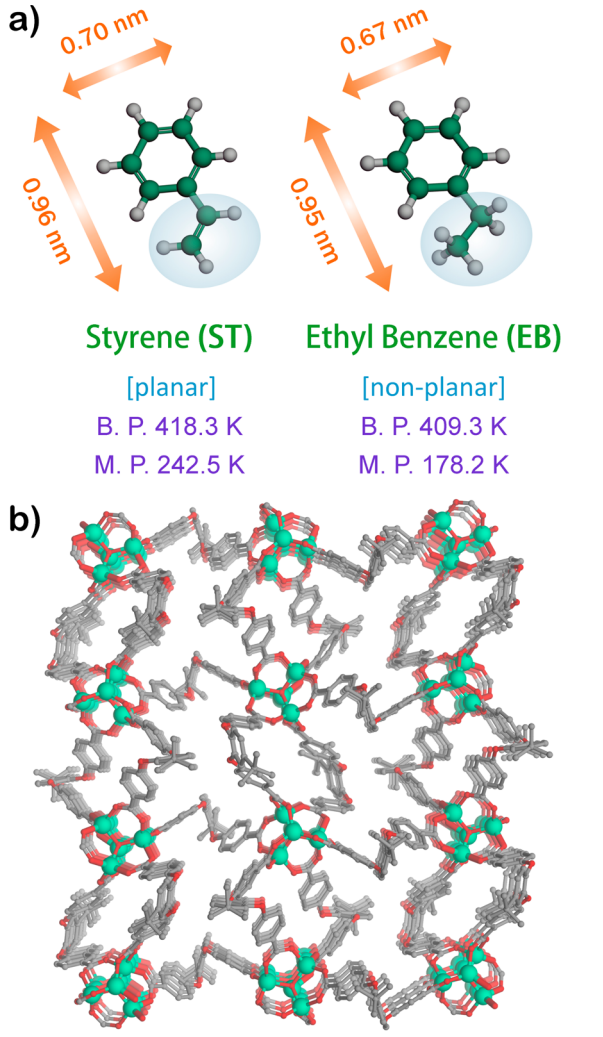

Figure 1. (a) Dimensions and relevant physical attributes of ST and EB molecules.[38] (b) Overall structure of compound **1** (desolvated squeezed framework) along crystallographic *a*-axis.

synthesized phase (**1⊃G**), accompanied by the loss of coordinated dimethylformamide (DMF) molecules and pore-closing event in single-crystal to single-crystal (SCSC) fashion. The prime focus of our current work is to demonstrate the outstanding potential of DynaMOF-100 for selective adsorption of ST from mixtures containing EB (Scheme 1). The effective mean pore diameter of 5.1 Å for flexible DynaMOF-100 facilitates selective entry of PX through pore opening but does not respond to the sterically demanding guests OX, MX, and EB (dimensional and bp closeness: Supporting Information, Figure S2). The salient dimension parameters MIN-1 and MIN-2 (Supporting Information, Table S4[32]) for ST are intriguingly quite similar to those of PX, with an even lower size of the adsorptive species as its minimum dimension (MIN-1). This factor, coupled with a strikingly close MIN-2 value of ST as compared to the host soft porous adsorbent DynaMOF-100, allows a definite room for restricted limiting allowance principle[18] to operate for the inspected pair ST/EB (Figure 1a and Supporting Information, Figure S3). This intriguing dimensional compatibility between the probe-adsorptive ST and the host adsorbent prompted us to systematically investigate such anticipated selectivity and separation performance of ST over EB. Styrene is a planar molecule, whereas EB is nonplanar, due to the ethyl group protruded from the planar phenyl ring (Scheme 1 and Figure 1a). Because of differences in their flatness, ST may be expected to exert stronger interactions with the framework walls of DynaMOF-100.

Scheme 1. Schematic Illustration of Guest-Responsive Framework Flexibility Demonstrating Selective ST Separation over EB

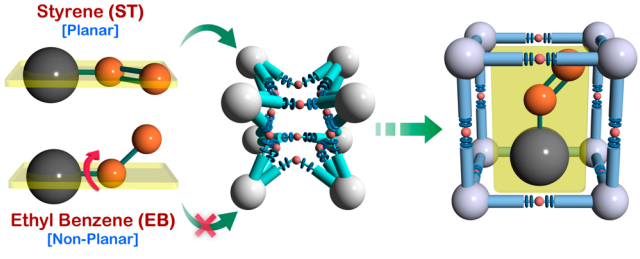

EXPERIMENTAL SECTION

Materials and Measurements. All the reagents and solvents were commercially available and used without further purification. Powder X-ray diffraction (PXRD) patterns were measured on Bruker D8 Advanced X-ray diffractometer at room temperature using Cu Kα radiation (λ = 1.5406 Å) with a scan speed of 0.5° min^{-1} and a step size of 0.01° in 2 θ. Thermogravimetric analysis (TGA) results were obtained in the temperature range of 30−800 °C on PerkinElmer STA 6000 analyzer under N_2 atmosphere, at a heating rate of 10 °C min^{-1}.

X-ray Structural Studies. Single-crystal X-ray data of compound **1⊃ST′** was collected at 100 K on a Bruker KAPPA APEX II CCD Duo diffractometer (operated at 1500 W power: 50 kV, 30 mA), using graphite-monochromated Mo Kα radiation (λ = 0.710 73 Å), mounted on nylon CryoLoops (Hampton Research) with Paraton-N (Hampton Research) oil. The data integration and reduction were processed with SAINT[33] software. A multiscan absorption correction was applied to the collected reflections. The structures were solved by the direct method using SHELXTL[34] and were refined on F^2 by full-matrix least-squares technique using the SHELXL-97[35] program package within the WINGX[36] program. All non-hydrogen atoms were refined anisotropically. All hydrogen atoms were located in successive difference Fourier maps, and they were treated as riding atoms using SHELXL default parameters. The structures were examined using the Adsym subroutine of PLATON[37] to ensure that no additional symmetry could be applied to the models. Supporting Information, Tables S5−S8 contain crystallographic data for the compound **1⊃ST′**. CCDC-983317, 983318, 983319, 1035236 (**1**, **1⊃PX′**, **1⊃G**, and **1⊃ST′**, respectively) along with Supporting Information contain the additional crystallographic information for these compounds.

Low-Pressure Gas Sorption Measurements. Low-pressure solvent sorption measurements were performed using BelAqua (Bel Japan). All the gases used were of 99.999% purity. As-synthesized crystals of compound **1⊃G** were heated at 180 °C under vacuum for 24 h, to get guest-free crystals of compound **1**. Prior to adsorption measurement, the guest-free sample **1** was pretreated at 170 °C under vacuum for 2 h, using BelPrepvacII, and purged with N_2 on cooling.

Solvent Exposure Study. Crystalline solid powder of compound **1** taken in smaller glass vials was kept open inside larger capped closed glass vials containing different guest solvents (ST and EB, respectively) over a period of 48 h to allow vapor-phase exposure of solvents and was characterized by PXRD.

Synthesis of Resolvated Phase {[$Zn_4O(L)_3(DMF)_2$]·(C_8H_8)$_3$}$_n$ (1⊃ST′). Colorless single crystals of **1⊃ST′** were obtained on exposing the crystals of **1** to the vapor of a solution of ST (2 mL) and DMF (1 mL) for 72 h, without allowing any disturbance of the system.

DOI: 10.1021/acs.inorgchem.5b00206
Inorg. Chem. 2015, 54, 4403−4408

RESULTS AND DISCUSSION

To verify the respective adsorptive uptake amounts, vapor sorption experiments for both the solvents ST and EB were recorded at 298 K. The sorption profile of ST came up with a gradual increase of uptake amount with steadily increasing pressure up to ~six molecules per formula unit (corresponding to ~86 mLg^{-1}), while, on the contrary, EB uptake amount was found to be only 0.63 molecules per formula unit (9.4 mL g^{-1}) (Figure 2 and Supporting Information, Figure S10). The

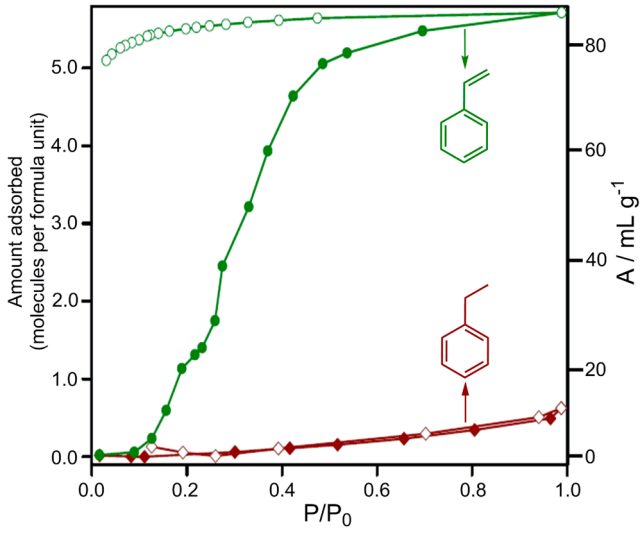

Figure 2. Solvent sorption isotherms for compound **1** recorded at 298 K for ST and EB. Closed and open symbols denote adsorption and desorption, respectively.

hysteresis in the ST isotherm, during the adsorption/desorption cycles, is a typical isotherm characteristic observed when guest-induced structural changes occur,[39] and a detailed quantitative analysis, such as that presented by Dubbeldam et al., is required for a quantitative understanding of the isotherms.[40]

This differential adsorption behavior toward these two related species consolidated that the framework flexibility of desolvated phase 1 allows the entry of the planar guest ST but not the nonplanar ones like EB, due to steric hindrance that originates in the case of the latter. The olefin-bond mediated extended conjugation for ST affords absolute planarity to this molecule, which sterically facilitates the selective uptake of ST. Bed regeneration for this material was verified by performing three consecutive cycles of ST adsorption with the same desolvated phase **1**, which registered excellent reproducibility features (Supporting Information, Figures S11 and S12).

The PXRD patterns and TGA profiles for the two phases (Supporting Information, Figures S6–S8), namely, **1⊃ST** and **1⊃EB**, precisely corroborate with the structural transformations occurring on the interplay of host–guest interactions. These results seemed to be in absolute agreement to those obtained from solvent sorption studies, since the characteristic PXRD pattern for **1** remained unaltered in case of **1⊃EB**, while exposure to ST marked a drastic change suggesting a clear phase transition. Interestingly enough, the PXRD pattern of **1⊃ST** registered a striking similarity to the phase **1⊃G**, referring to a breathing phenomenon that might have occurred on ST exposure. In fact, TGA results simultaneously affirmed this observation, since no significant weight loss accompanied the exposure-mediated phase **1⊃EB**, while **1⊃ST** registered a substantial ~25% weight loss. As an ancillary reinforcement supporting the selective interplay of ST with the flexible framework **1** as compared to EB, ^{13}C NMR experiments with the DCl/deuterated dimethyl sulfoxide digested samples after vapor exposure to these two different solvent vapors (Supporting Information, Figure S13) were performed, which indisputably presented barely the characteristic ST signals.

To verify the separation-viability in actuality, phase **1** was immersed into solvents ST, EB, and binary mixture solution of ST/EB (1:1) for 3 h, and the respective amounts of the nonadsorbed isomers were scanned by gas chromatography (GC) at specific intermediate time intervals. The detailed description of the GC experiment with the supernatant solvent(s) is provided in the Supporting Information. Ensuing results (Figure 3 and Supporting Information, Figures S14–S17) evidently authenticate that the observed decline in the characteristic signal intensity is exclusively due to the contribution of ST; the gradually diminishing intensity trend steadily tells the difference with increasing immersion time of DynaMOF-100.

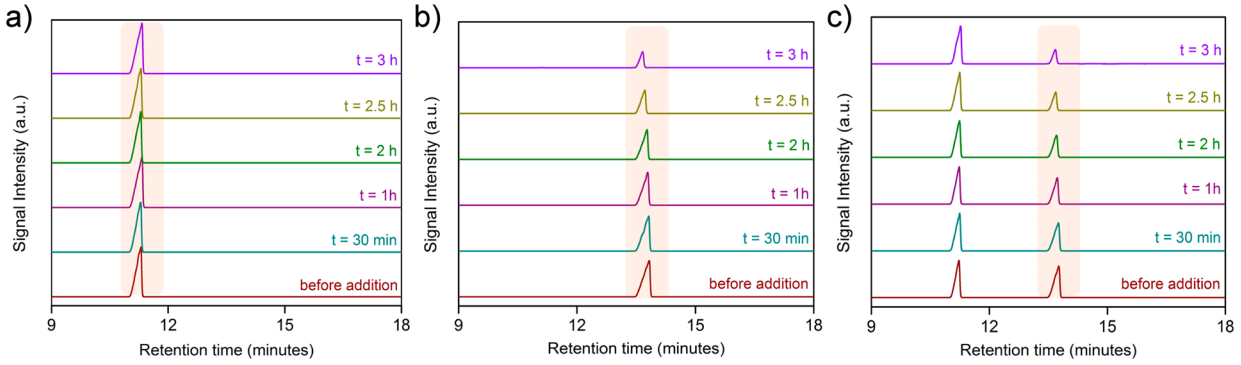

Figure 3. (a) GC chromatogram of the supernatant solutions recorded at the specified time intervals in the setup A (EB immersion test). Highlighted signals denote the contribution of EB only, intensity of which is remaining unchanged with increasing time of immersion with MOF, (b) GC chromatogram of the supernatant solutions recorded at the specified time intervals in the setup B (ST immersion test). Highlighted signals denote the contribution of ST only, intensity of which is getting steadily diminished with increasing time of immersion with MOF, (c) GC chromatogram of the supernatant solutions recorded at the specified time intervals in the setup C (ST/EB mixture immersion test). Highlighted region denotes the individual signal for the contribution of ST only, intensity of which is getting steadily diminished with increasing MOF immersion-time.

DOI: 10.1021/acs.inorgchem.5b00206
Inorg. Chem. 2015, 54, 4403–4408

We now evaluate EB/ST separations using the ideal adsorbed solution theory (IAST) calculations. Figure 4a shows the experimental data for pure component isotherms for EB and ST in DynaMOF-100; the continuous solid lines are Langmuir–Freundlich fits; the parameters are specified in Supporting Information, Table S3.

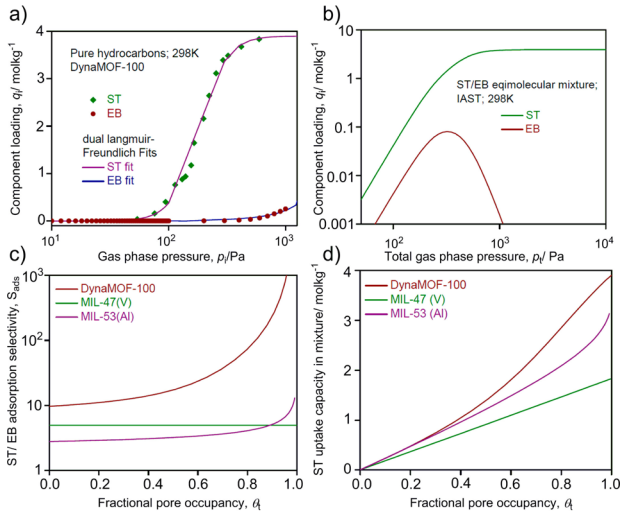

Figure 4. (a) Comparison of experimental data for pure component isotherms for EB and ST in DynaMOF-100 with Langmuir–Freundlich fits that are shown by the continuous solid lines; (b) IAST calculations for ST/EB adsorption selectivity for equimolar ST(1)/EB(2) mixtures in DynaMOF-100; (c) IAST calculations for ST/EB adsorption selectivity for equimolar ST(1)/EB(2) mixtures in MIL-47(V), MIL-53(Al), and DynaMOF-100. The x-axis is fractional occupancy θ_t within the pores of the MOFs; (d) IAST calculations for ST uptake capacity for equimolar ST(1)/EB(2) mixtures in MIL-47(V), MIL-53(Al), and DynaMOF-100. The x-axis is fractional occupancy θ_t within the pores of the MOFs.

Figure 4b shows IAST calculations for ST/EB adsorption selectivity, S_{ads}, for equimolar ST(1)/EB(2) mixtures in DynaMOF-100.

$$S_{ads} = \frac{q_1/q_2}{p_1/p_2} \tag{1}$$

We note that, for pressures exceeding ~1 kPa, the adsorbed phase contains predominantly ST. The high ST/EB selectivities as evidenced in Figure 4b,c are caused by better molecular packing of the planar ST molecules within the MOF channels. The mechanism of separation due to molecular packing effects of mixtures of aromatics is particularly strong for operation under pore saturation conditions, as has been explained in literature.[40] We see, from Figure 4, that pore saturation is also attained at pressures exceeding 1 kPa and ambient temperatures. It is anticipated that industrial separations in fixed-bed adsorbers will operate under conditions approaching pore saturation.[41] For this reason we define the fractional occupancy

$$\theta_t = \sum_{i=1}^{n} \frac{q_i}{q_{i,sat}} \tag{2}$$

Figure 4c presents a comparison the adsorption selectivities of DynaMOF-100 with MIL-47(V) and MIL-53(Al) as a function of the fractional pore occupancy. We note that the value of S_{ads} for DynaMOF-100 is ca. 1 to 2 orders of magnitude higher than that of MIL-47(V) and MIL-53(Al). Figure 4d shows IAST calculations for ST uptake capacity for equimolar ST(1)/EB(2) mixtures in MIL-47(V), MIL-53(Al), and DynaMOF-100. The uptake capacity of DynaMOF-100 is significantly higher than that of the other two MOFs. Because of the significantly higher adsorption selectivity and higher capacity we should expect that sharp separations of ST(1)/EB(2) mixtures is realized in a fixed-bed adsorber.

While repeated trials were attempted to obtain the crystal structure of this resolvated phase, an analogous phase **1⊃ST′** (Supporting Information, Figures S1 and S4; as indicated from the exactly alike PXRD patterns for both, Supporting Information, Figure S9) was obtained on exposing the crystals of **1** to the vapor of a binary mixture solution of ST (2 mL) and DMF (1 mL) for 72 h. SC-XRD analysis of this novel compound **1⊃ST′** (formula: $\{[Zn_4O(L)_3(DMF)_2]\cdot(C_8H_8)_3\}_n$) disclosed that the nearly similar unit cell parameters to those of the crystals of **1⊃G** and crystallized in monoclinic centrosymmetric space group $P21/c$ (Supporting Information, Table S5). As an unambiguous conclusive evidence of selective interplay of ST accompanying this solid-state dynamic structural transformation, ST molecules could be clearly located in the SC-XRD structure for the **1⊃ST′** phase crystals, residing inside the porous channels of the host framework (Figures 5 and Supporting Information, Figures S24 and S25). This could only be possible after commensurate stacking-mediated accommodation of the planar ST molecules inside the

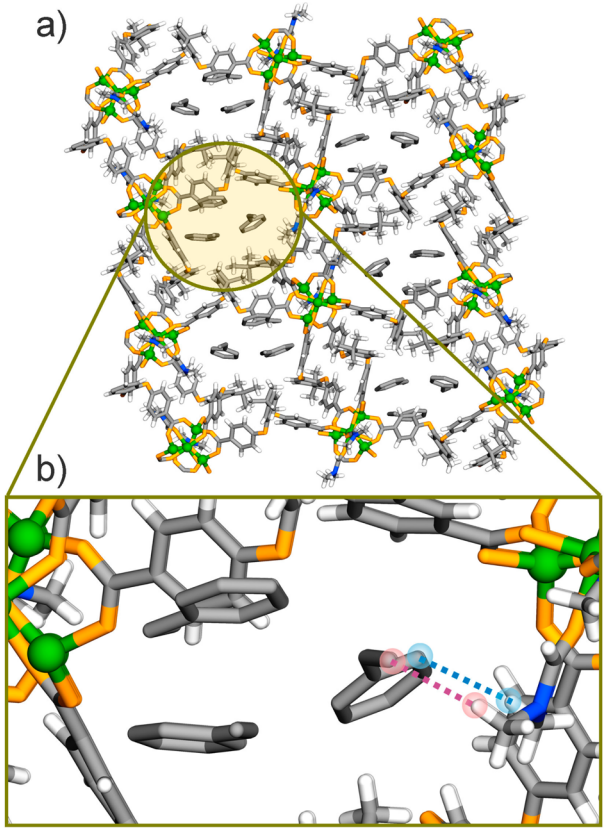

Figure 5. (a) Overall structure of resolvated phase **1⊃ST′**, with free guest ST molecular species accommodated inside the channels, along crystallographic a-axis. (b) Enlarged view of one of these channels showing noncovalent interactions (representative) between the host MOF and guest ST species by dotted lines.

DOI: 10.1021/acs.inorgchem.5b00206
Inorg. Chem. 2015, 54, 4403–4408

hydrophobic channels of the shrinked windows of desolvated framework **1**; prominent noncovalent interactions are observed between the host MOF channel and the guest ST, as represented in Figure 5b.

Subsequent to the phase purity-confirmation for the new phase **1⊃ST′** from PXRD (Supporting Information, Figure S9), both TGA and PXRD analyses for the two phases, namely, **1⊃ST** and **1⊃ST′**, confirmed their similar nature (Supporting Information, Figures S7 and S9). To check reversibility of this ST inclusion, the crystals of **1⊃ST′** were heated at 160 °C under reduced pressure for 3 h, to obtain the desolvated phase **1″** (DynaMOF-100). TGA and PXRD profiles (Supporting Information, Figures S7 and S9) confirmed the resemblance with the pristine desolvated phase **1**, confirming the ST-inclusion reversibility.

CONCLUSION

In the work reported here, the framework flexibility of DynaMOF-100 has been strategically exploited for achieving selective ST uptake over EB. The separation relies on the closeness in the dimensions of the guest ST molecule and the host material. DynaMOF-100 exhibits significant framework flexibility because of its constituent adjustable ether nodes, which precisely mediates the guest inclusion, accompanied by solid-state structural transformations. IAST calculations for separation of EB/ST mixtures have shown a significant superiority of DynaMOF-100 when compared to the only two reported MOFs, namely, MIL-47(V) and MIL-53(Al). Moreover, aimed at potentially significant separation of OX/MX/PX/EB mixtures, DynaMOF-100 is also found to be significantly superior to both MAF-X8 and BaX zeolite. The strategy of using guest-selective structural transformations of the MOF frameworks could be proficiently exploited for other industrially important separations of mixtures of aromatic molecules, especially hydrocarbons.

ASSOCIATED CONTENT

Supporting Information

Microscopy images, dimensions of molecules, asymmetric units for phases, progression of single 2D sheet, TGA plots, PXRD patterns, solvent sorption isotherms, ^{13}C spectra, GC chromatogram, comparison of experimental isotherm data, breakthrough simulations, IAST calculations, packed bed adsorber schematic, pulse chromatographic simulation, resolvated framework, perspective view of phase, Langmuir–Freundlich parameters, crystallographic data table. This material is available free of charge via the Internet at http://pubs.acs.org.

AUTHOR INFORMATION

Corresponding Author

*Fax: +91 20 2590 8186. E-mail: sghosh@iiserpune.ac.in. Home page: http://www.iiserpune.ac.in/~sghosh/.

Author Contributions

The manuscript was written through contributions of all authors.

Notes

The authors declare no competing financial interest.

ACKNOWLEDGMENTS

We are grateful to IISER Pune for research facilities. DST (Project No.GAP/DST/CHE-12-0083) is acknowledged for the financial support. S.M. and A.V.D. thank IISER Pune for research fellowship. B.J. and B.M. are thankful to CSIR for research fellowship. We acknnowledge Dr. C. E. Webster of Mississippi State Univ. for helping to calculate the relevant dimensions for ST and Dr. R. Saha for crystllographic analysis.

REFERENCES

(1) *Kirk-Othmer Encyclopedia of Chemical Technology;* John Wiley & Sons, Inc.: New York, 2008; pp 1040.
(2) *Ullmann's Encyclopedia of Industrial Chemistry,* 6th ed.; John Wiley & Sons, Inc.: New York, 2006; electronic release.
(3) He, Y.; Krishna, R.; Chen, B. *Energy Environ. Sci.* **2012**, *5*, 9107–9120.
(4) Gu, Z.-Y.; Yang, C.-X.; Chang, N.; Yan, X.-P. *Acc. Chem. Res.* **2012**, *45*, 734–745.
(5) Vermoortele, F.; Maes, M.; Moghadam, P. Z.; Lennox, M. J.; Ragon, F.; Boulhout, M.; Biswas, S.; Laurier, K. G. M.; Beurroies, I.; Denoyel, R.; Roeffaers, M.; Stock, N.; Düren, T.; Serre, C.; De Vos, D. E. *J. Am. Chem. Soc.* **2011**, *133*, 18526–18529.
(6) Finsy, V.; Verelst, H.; Alaerts, L.; Vos, D. De; Jacobs, P. A.; Baron, G. V.; Denayer, J. F. M. *J. Am. Chem. Soc.* **2008**, *130*, 7110–7118.
(7) Krishna, R.; van Baten, J. M. *Phys. Chem. Chem. Phys.* **2011**, *13*, 10593–10616.
(8) Bárcia, P. S.; Zapata, F.; Silva, J. A. C.; Rodrigues, A. E.; Chen, B. *J. Phys. Chem. B* **2007**, *111*, 6101–6103.
(9) Rowsell, J. L. C.; Yaghi, O. M. *Microporous Mesoporous Mater.* **2004**, *73*, 3–14.
(10) Rosseinsky, M. J. *Microporous Mesoporous Mater.* **2004**, *73*, 15–30.
(11) Butler, J. R.; Watson, J. M.; Forward, C. H. U.S. Patent 4417085, 1983.
(12) Berg, L. U.S. Patent 4959128, 1990.
(13) Alaerts, L.; Kirschhock, C. E. A.; Maes, M.; van der Veen, M. A.; Finsy, V.; Depla, A.; Martens, J. A.; Baron, G. V.; Jacobs, P. A.; Denayer, J. F. M.; De Vos, D. E. *Angew. Chem., Int. Ed.* **2007**, *46*, 4293–4297.
(14) Peralta, D.; Chaplais, G.; Simon-Masseron, A.; Barthelet, K.; Chizallet, C.; Quoineaud, A.-A.; Pirngruber, G. D. *J. Am. Chem. Soc.* **2012**, *134*, 8115–8126.
(15) Stylianou, K. C.; Rabone, J.; Chong, S. Y.; Heck, R.; Armstrong, J.; Wiper, P. V.; Jelfs, K. E.; Zlatogorsky, S.; Bacsa, J.; McLennan, A. G.; Ireland, C. P.; Khimyak, Y. Z.; Thomas, K. M.; Bradshaw, D.; Rosseinsky, M. J. *J. Am. Chem. Soc.* **2012**, *134*, 20466–20478.
(16) Lusi, M.; Barbour, L. J. *Angew. Chem., Int. Ed.* **2012**, *51*, 3928–3931.
(17) Peralta, D.; Chaplais, G.; Paillaud, J.-L.; Simon-Masseron, A.; Barthelet, K.; Pirngruber, G. D. *Microporous Mesoporous Mater.* **2013**, *173*, 1–5.
(18) Mukherjee, S.; Joarder, B.; Manna, B.; Desai, A. V.; Chaudhari, A. K.; Ghosh, S. K. *Sci. Rep.* **2014**, *4*, 5761 DOI: 10.1038/srep05761.
(19) Herm, Z. R.; Wiers, B. M.; Mason, J. A.; van Baten, J. M.; Hudson, M. R.; Zajdel, P.; Brown, C. M.; Masciocchi, N.; Krishna, R.; Long, J. R. *Science* **2013**, *340*, 960–964.
(20) Peralta, D.; Chaplais, G.; Simon-Masseron, A.; Barthelet, K.; Pirngruber, G. D. *Ind. Eng. Chem. Res.* **2012**, *51*, 4692–4702.
(21) Finsy, V.; Calero, S.; García-Pérez, E.; Merkling, P. J.; Vedts, G.; De Vos, D. E.; Baron, G. V.; Denayer, J. F. M. *Phys. Chem. Chem. Phys.* **2009**, *11*, 3515–3521.
(22) Bárcia, P. S.; Guimarães, D.; Mendes, P. A.P.; Silva, J. A.C.; Guillerm, V.; Chevreau, H.; Serre, C.; Rodrigues, A. E. *Microporous Mesoporous Mater.* **2011**, *139*, 67–73.
(23) Cychosz, K.; Wong-Foy, A.; Matzger, A. *J. Am. Chem. Soc.* **2009**, *131*, 14538–14543.
(24) Gu, Z.; Yan, X. *Angew. Chem.* **2010**, *122*, 1519–1522; *Angew. Chem., Int. Ed.* **2010**, *49*, 1477–1480.

DOI: 10.1021/acs.inorgchem.5b00206
Inorg. Chem. 2015, 54, 4403–4408

(25) Alaerts, L.; Maes, M.; Giebeler, L.; Jacobs, P. A.; Martens, J. A.; Denayer, J. F. M.; Kirschhock, C. E. A.; De Vos, D. E. *J. Am. Chem. Soc.* **2008**, *130*, 14170−14178.
(26) Joarder, B.; Mukherjee, S.; Chaudhari, A. K.; Desai, A. V.; Manna, B.; Ghosh, S. K. *Chem.—Eur. J.* **2014**, *20*, 15303−15308.
(27) Shimomura, S.; Horike, S.; Matsuda, R.; Kitagawa, S. *J. Am. Chem. Soc.* **2007**, *129*, 10990−10991.
(28) Maes, M.; Vermoortele, F.; Alaerts, L.; Couck, S.; Kirschhock, C. E. A.; Denayer, J. F. M.; De Vos, D. E. *J. Am. Chem. Soc.* **2010**, *132*, 15277−15285.
(29) Remy, T.; Ma, L.; Maes, M.; De Vos, D. E.; Baron, G. V.; Denayer, J. F. M. *Ind. Eng. Chem. Res.* **2012**, *51*, 14824−14833.
(30) Maes, M.; Vermoortele, F.; Boulhout, M.; Boudewijns, T.; Kirschhock, C.; Ameloot, R.; Beurroies, I.; Denoyel, R.; De Vos, D. E. *Microporous Mesoporous Mater.* **2012**, *157*, 82−88.
(31) Torres-Knoop, A.; Krishna, R.; Dubbeldam, D. *Angew. Chem., Int. Ed.* **2014**, *53*, 7774−7778.
(32) Webster, C. E.; Drago, R. S.; Zerner, M. C. *J. Am. Chem. Soc.* **1998**, *120*, 5509−5516.
(33) *SAINT Plus,* Version 7.03; Bruker AXS Inc.: Madison, WI, 2004.
(34) Sheldrick, G. M. *SHELXTL Reference Manual,* Version 5.1; Bruker AXS: Madison, WI, 1997.
(35) Sheldrick, G. M. *Acta Crystallogr., Sect. A* **2008**, 112−122.
(36) Farrugia, L. *WINGX,* Version 1.80.05; University of Glasgow: Glasgow, Scotland, 2015.
(37) Spek, A. L. *PLATON, A Multipurpose Crystallographic Tool;* Utrecht University: Utrecht, The Netherlands, 2005.
(38) Torres-Knoop, A.; Heinen, J.; Krishna, R.; Dubbeldam, D. *Langmuir* **2015**, *31*, 3771−3778.
(39) Serre, C.; Millange, F.; Thouvenot, C.; Nouguès, M.; Marsolier, G.; Louër, D.; Férey, G. *J. Am. Chem. Soc.* **2002**, *124*, 13519−13526.
(40) Dubbeldam, D.; Krishna, R.; Snurr, R. Q. *J. Phys. Chem. C* **2009**, *113*, 19317−19327.
(41) Krishna, R. *Phys. Chem. Chem. Phys.* **2015**, *17*, 39−59.

DOI: 10.1021/acs.inorgchem.5b00206
Inorg. Chem. 2015, 54, 4403−4408

Supplementary Information for

Exploiting Framework Flexibility of a Metal-Organic Framework for Selective Adsorption of Styrene over Ethylbenzene

Soumya Mukherjee,[1] Biplab Joarder,[1] Aamod V. Desai,[1] Biplab Manna,[1] Rajamani Krishna,[2] and Sujit K. Ghosh[1*]

[1] Indian Institute of Science Education and Research (IISER), Dr. Homi Bhabha Road, Pashan, Pune-411008, India
[2] Van 't Hoff Institute for Molecular Sciences, University of Amsterdam, Science Park 904, 1098 XH Amsterdam, The Netherlands
Tel: +91-20-2590 8076; Fax: +91-20-2590 8186; E-mail: sghosh@iiserpune.ac.in

Table of Contents

Page no.

Figure S1: Microscopy images of crystalline phases 1⊃G, 1 and 1⊃ST' **S3**

Figure S2: Dimensions of the C_8-alkyl aromatic xylene isomers **S3**

Figure S3: Box dimensions for ST and EB molecule **S4**

Figure S4: Asymmetric Units for the phases 1 and 1⊃ST' **S5**

Figure S5: Progression of a single 2D-sheet (along *c*-axis) for the phase 1 **S5**

Figure S6-7: TGA plots for different 1⊃ solvent phases and phase 1, 1'' **S6**

Figure S8: PXRD patterns of 1⊃G, 1, 1⊃EB, 1⊃ST and 1⊃ST' (simulated) **S7**

Figure S9: PXRD patterns of 1⊃ST' (simulated), 1⊃ST' (experimental), 1⊃ST (experimental), 1⊃EB (experimental) and 1 (experimental) **S8**

Figure S10: Solvent sorption isotherms (ST and EB) at 298K **S9**

Figure S11: Reproducibility of ST sorption isotherm **S10**

Figure S12: Bar diagram representation of the ST-sorption reproducibility **S11**

Figure S13: ^{13}C NMR spectra for 1⊃ST and 1⊃EB **S12**

Figure S14-16: GC chromatogram for binary ST/EB mixture test **S13-16**

Figure S17: GC chromatogram of DynaMOF-100 after binary ST/EB mixture immersion test **S17**

Figure S18: Comparison of experimental data for pure component isotherms for ethylbenzene and styrene in MIL-47(V) and MIL-53(Al) **S22**

Figure S19: Breakthrough simulations for ethylbenzene/styrene mixtures in (a) MIL-47(V), and (b) MIL-53(Al) at 298 K **S22**

Figure S20: IAST calculations performed on DynaMOF-100 for xylenes **S23**

Figure S21: IAST calculations for xylenes on DynaMOF-100 against MAF-X8 and BaX Zeolite **S24**

Figure S22: Schematic of a packed bed adsorber **S25**

Figure S23: Pulse chromatographic simulation and transient breakthrough simulation results on DynaMOF-100 for xylene isomers **S25**

Figure S24: Resolvated framework 1⊃ST' on ST accommodation **S26**

Figure S25: Perspective view of 1⊃ST' phase **S27**

Table S1. Langmuir-Freundlich parameters for EB and ST at 298 K in MIL-47(V) **S28**

Table S2. Langmuir-Freundlich parameters for EB and ST at 298 K in MIL-53(Al) **S28**

Table S3: Dual-site Langmuir-Freundlich parameters for aromatic hydrocarbons **S29**

Table S4: Dimensions of Adsorptive molecules (Å) **S30**

Table S5: Crystallographic data table **S31**

Notations **S32-S33**

References **S34**

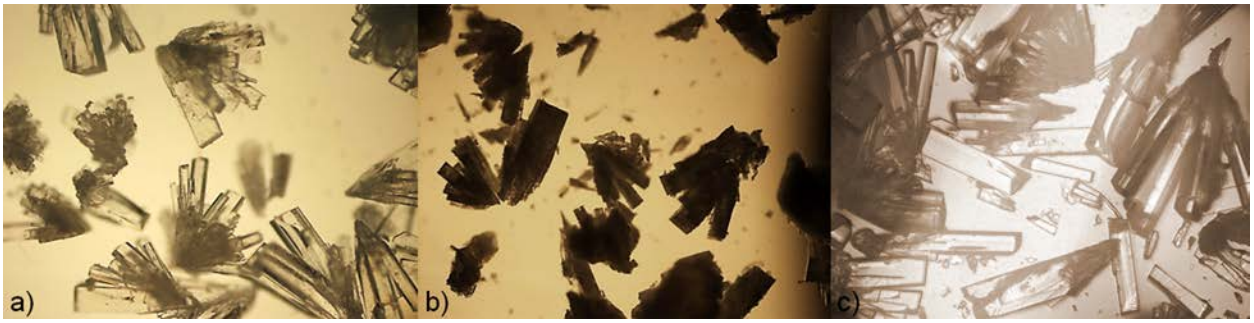

Figure S1. Microscopy images of the crystals for the different SCSC phases: a) compound **1⊃G** (as-synthesized), b) compound **1** (desolvated), c) compound **1⊃ST'**.

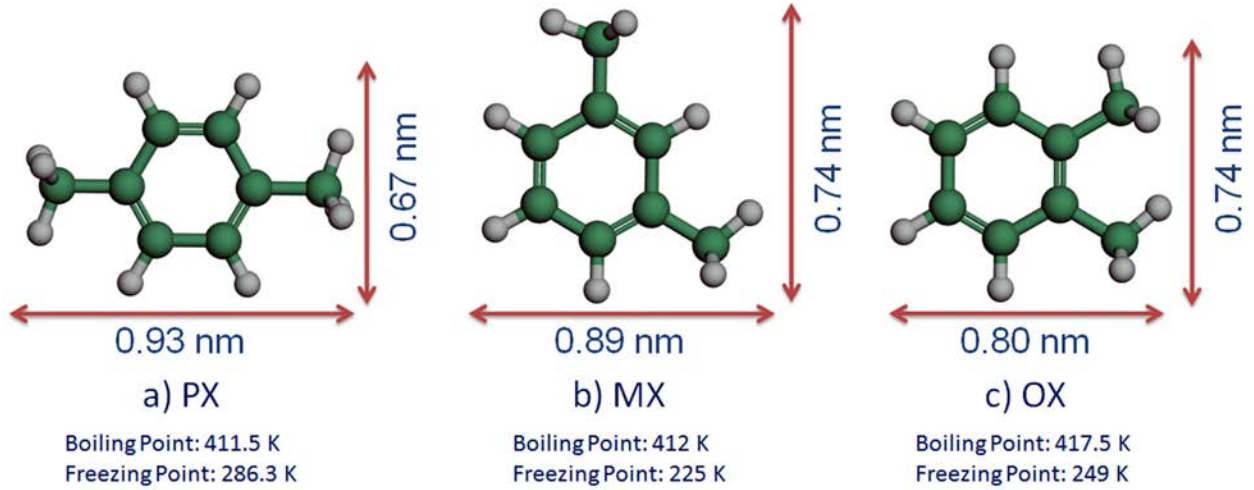

Figure S2. Dimensions of the C_8-alkyl aromatic xylene isomers (excluding ethyl benzene).

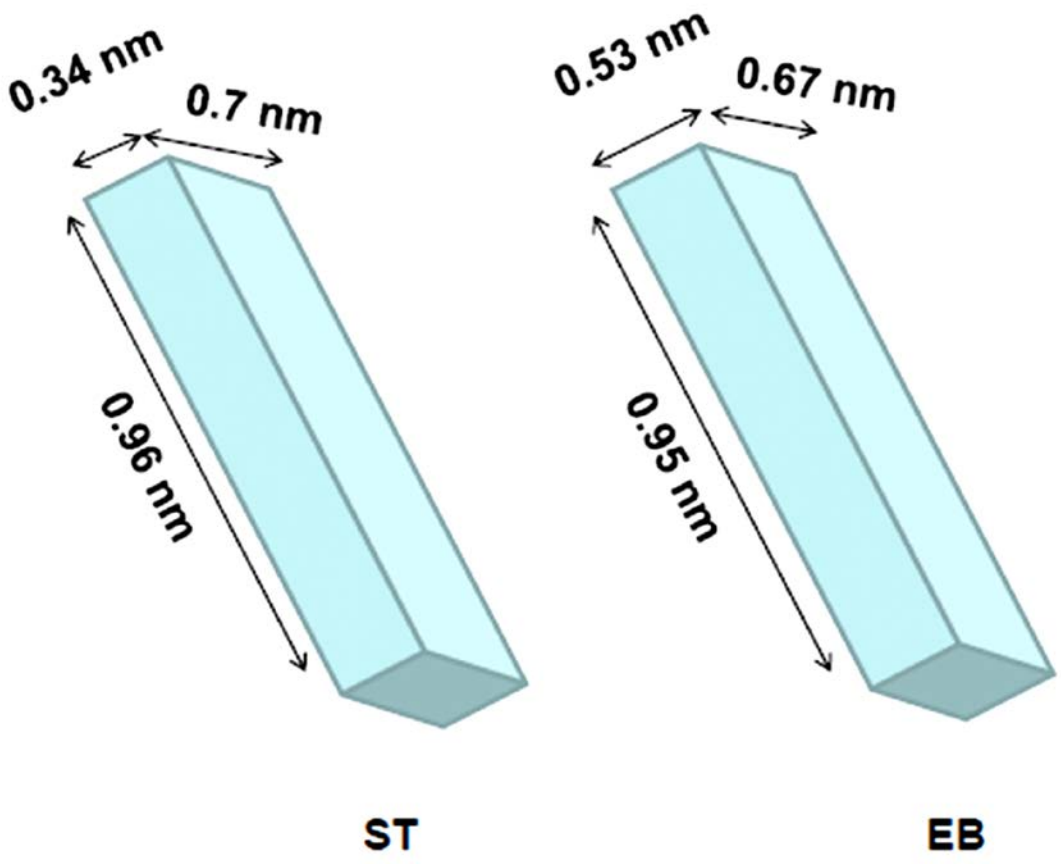

Figure S3. Box dimensions for ST and EB adsorptive molecules.

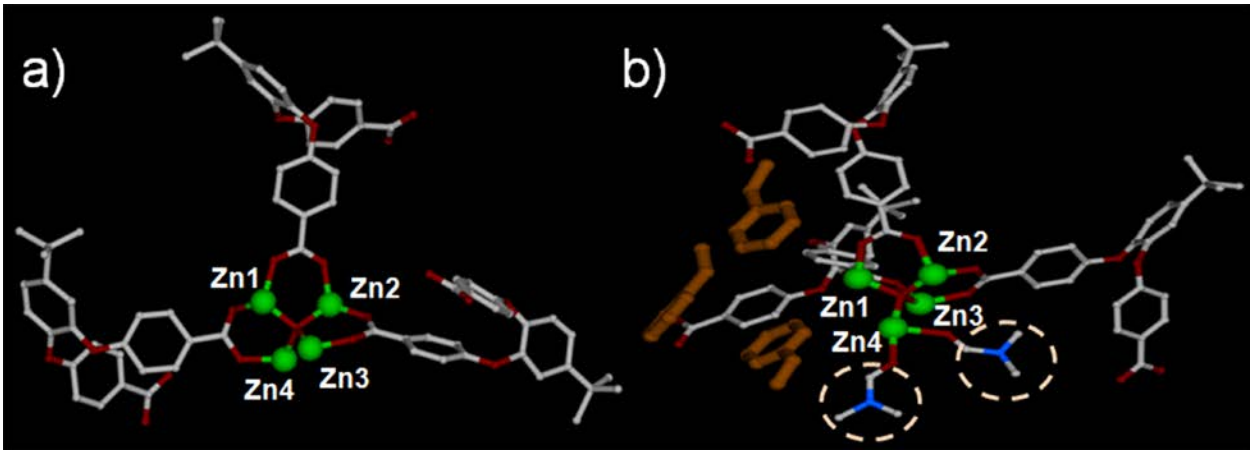

Figure S4. Asymmetric units for the two phases: a) Compound **1**, and b) Compound **1⊃ST'**; coordinated DMF molecules have been shown using circles (both coordinated to Zn4), with three ST molecules getting accommodated per asymmetric unit (as shown in yellow color for clarity).

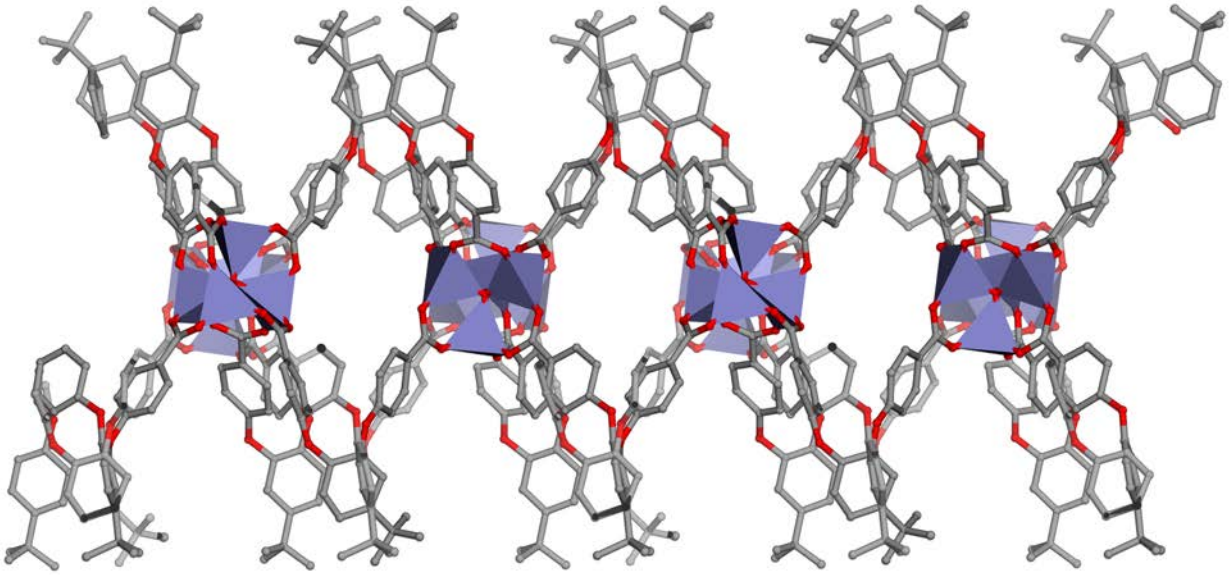

Figure S5. Progression of a single 2D-sheet (along *c*-axis) for the phase **1**.

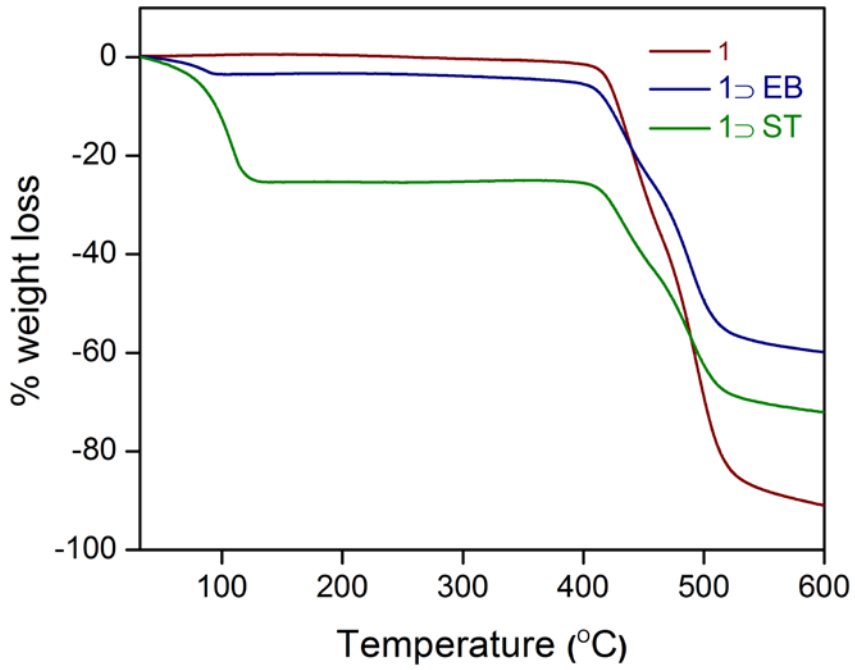

Figure S6. TGA plots for the guest-exposed phases of **1** (**1⊃ solvent**), compared with that of **1** (wine). Vapour of two solvents namely, **styrene** (olive), and **ethyl benzene** (navy) were exposed to obtain the phases **1⊃ST** and **1⊃EB** respectively.

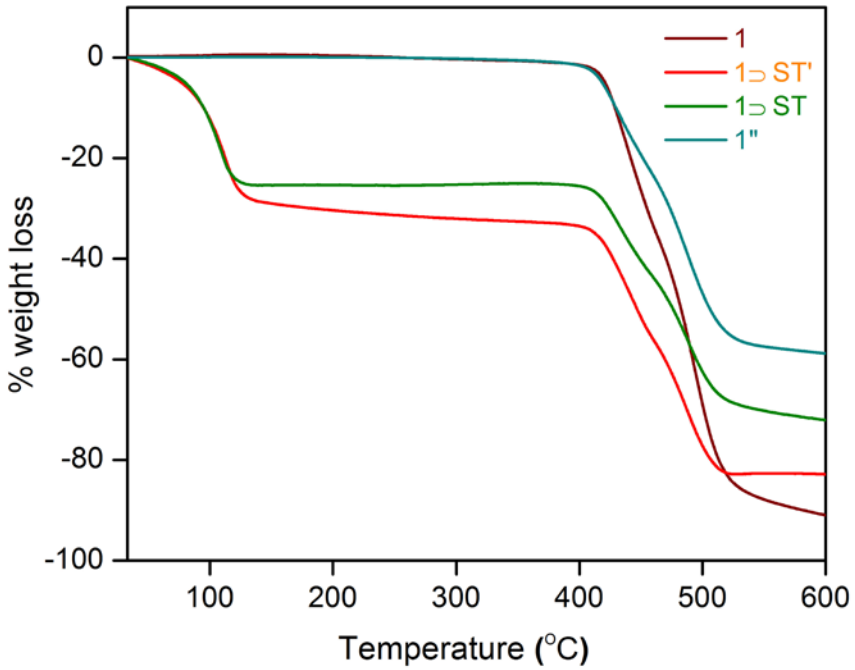

Figure S7. TGA plots for desolvated phase **1** (wine), compared with that of ST-exposed sample **1⊃ST** (purple), crystals **1⊃ST'**, along with the heated (redesolvated) phase **1''**.

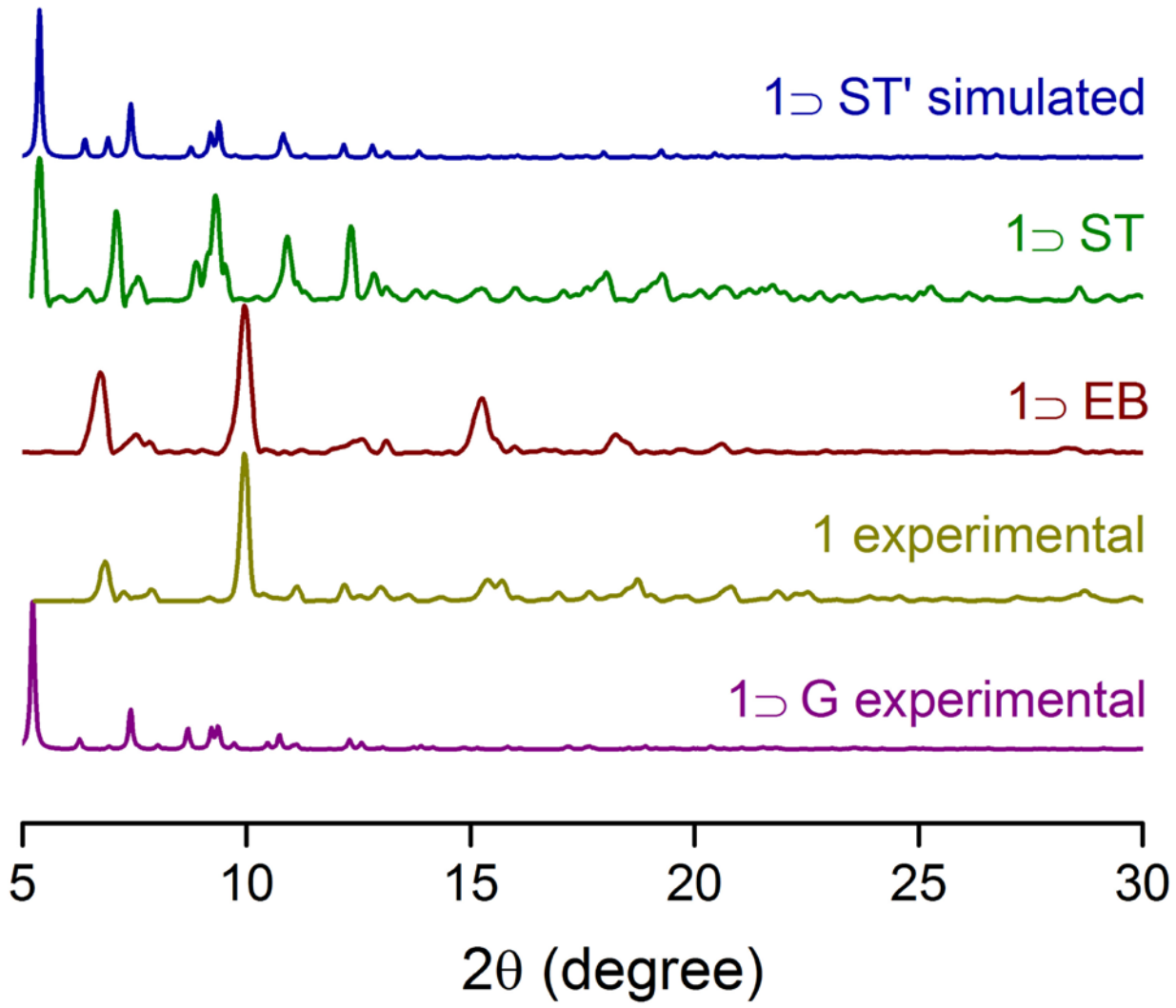

Figure S8. Experimental PXRD patterns of **1⊃G**, **1**, **1⊃EB, 1⊃ST** plotted with the simulated PXRD pattern of **1⊃ST'**.

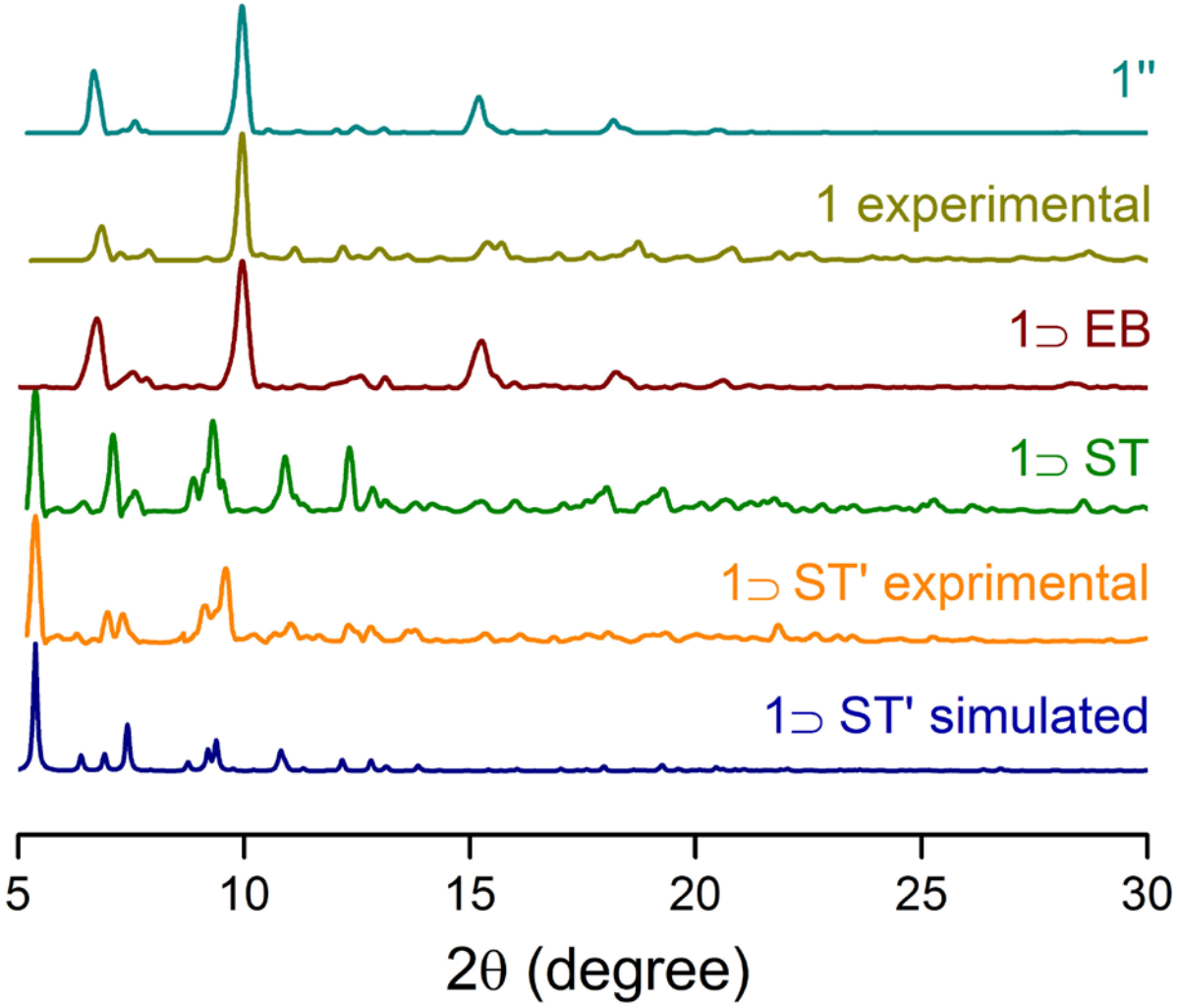

Figure S9. Powder X-ray diffraction (PXRD) patterns of compounds **1⊃ST'** (simulated), **1⊃ST'** (experimental), **1⊃ST** (experimental), **1⊃EB** (experimental), **1** (desolvated phase' experimental) and **1**".

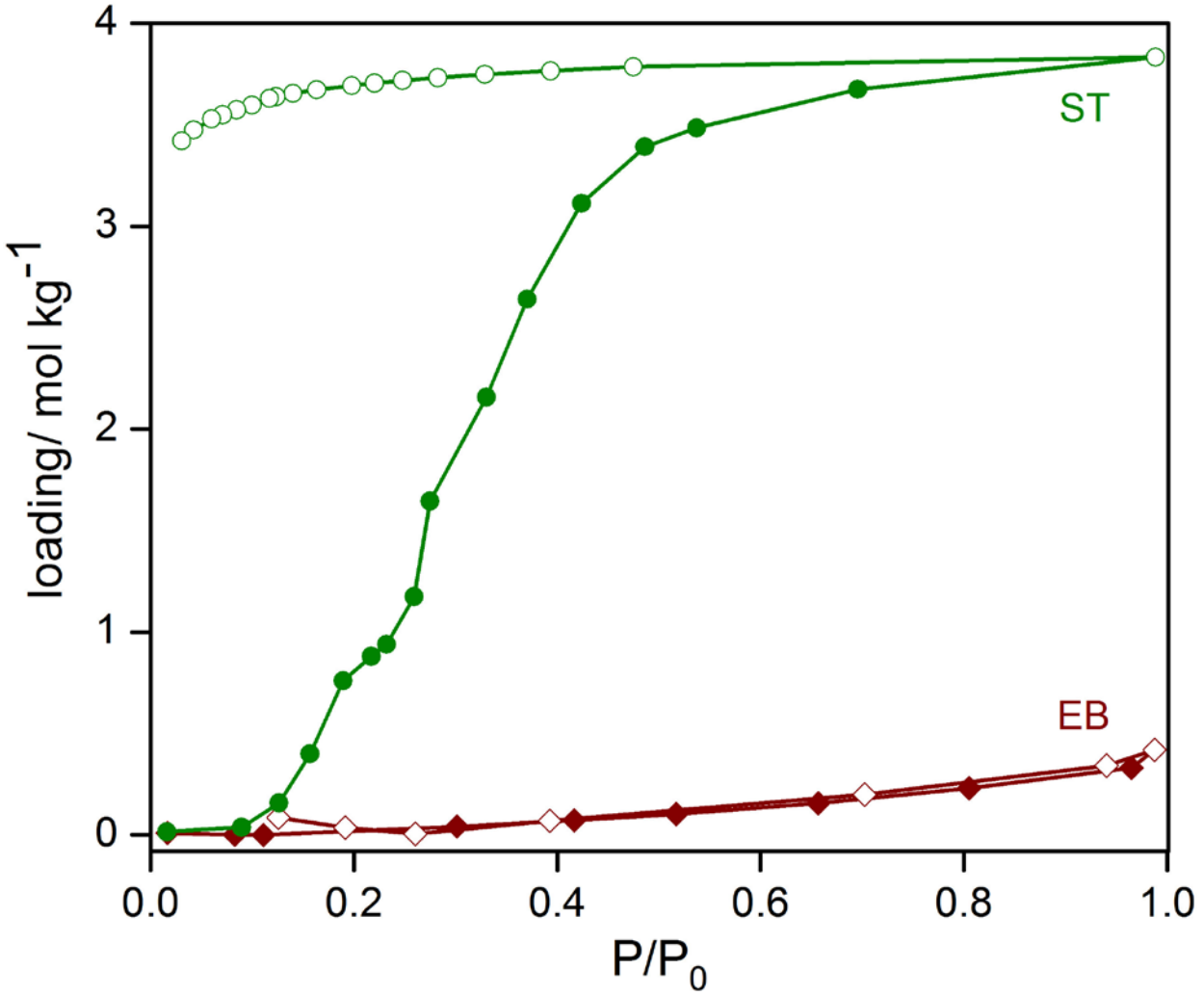

Figure S10. Single component adsorption isotherms for styrene and ethyl benzene in terms of loading (mol kg^{-1}) against increasing relative pressure.

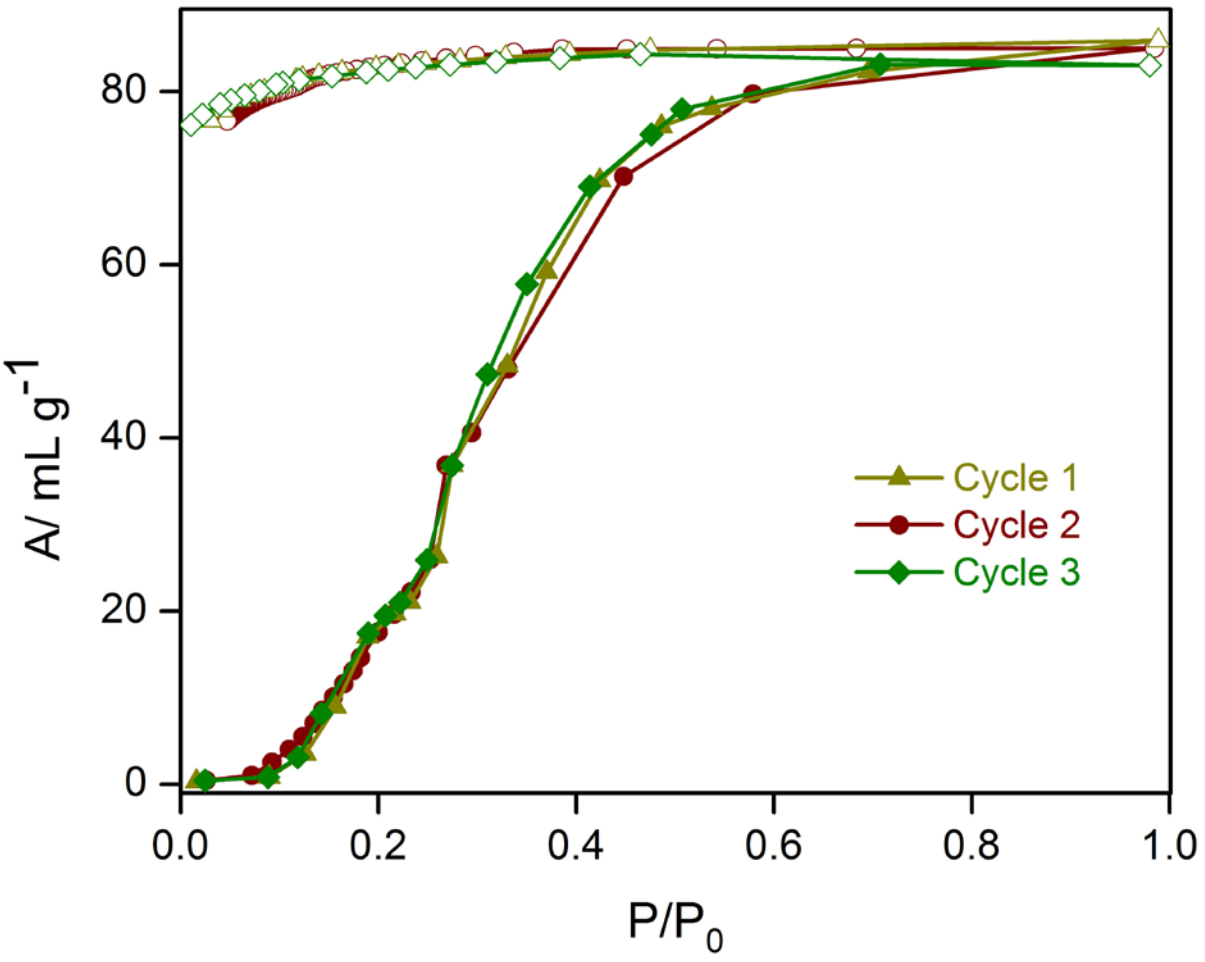

Figure S11: The recyclability of the ST adsorption behavior was confirmed by reproducing the same isotherm on unchanged desolvated sample **1** for three consecutive cycles at 298 K. Filled shapes: adsorption, hollow shapes: desorption.

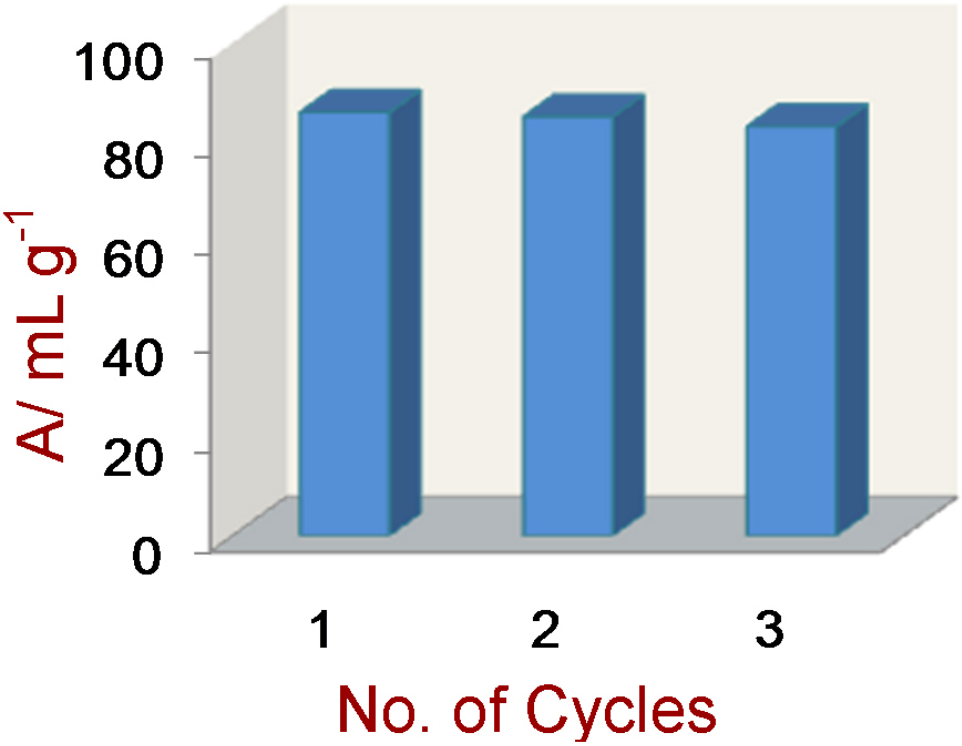

Figure S12: Bar diagram representation of the recyclability for the ST adsorption behavior as confirmed by reproducing the same isotherm on unchanged desolvated sample **1** for three consecutive cycles at 298 K. Similar amounts of ST-uptake suggests the ST-sorption's recyclability behaviour for the material **1**.

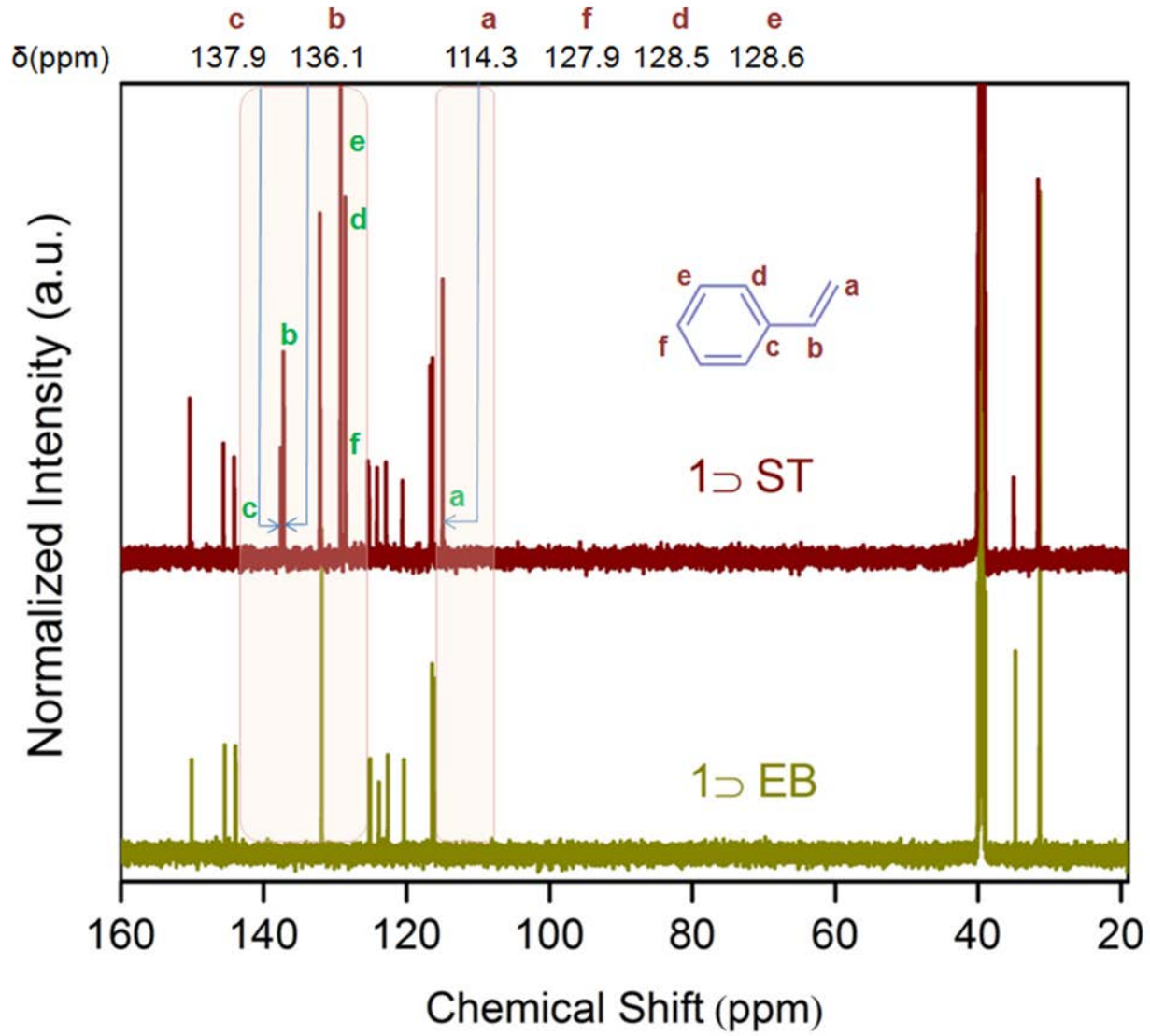

Figure S13. ^{13}C NMR spectra for styrene and ethyl benzene vapor-exposed phases of compound **1**. Vapor of each of these two solvents were exposed for 48h to the phase **1** before digesting in DCl/DMSO- d_6.

GC experiment to verify styrene-selectivity: Crystalline phase **1** (100 mg) was immersed into singular and/or mixture solutions of styrene/ethyl benzene for 3 h according to the following three different combinations, and GC chromatogram were recorded by pipetting out the supernatant solutions (0.123 mL each time) at regular time intervals, and preparing the GC samples in 1.3 mL MeCN in each of the occurrences. (GC parameters employed are mentioned after the description of the three setups.)

Setup A: Ethyl benzene immersion test: 100 mg of **1** was kept immersed in a solution of EB (3mL) for 1h, while in the intermediate time intervals 0.123 mL of the supernatant solution were pipetted out for recording the GC chromatogram at those respective times (Fig. S14).

Setup B: Styrene immersion test: 100 mg of **1** was kept immersed in a solution of ST (3mL) for 1h, while in the intermediate time intervals 0.123 mL of the supernatant solution were pipetted out for recording the GC chromatogram at those respective times (Fig. S15).

Setup C: Binary styrene/ethyl benzene (1:1) mixture immersion test: 100 mg of **1** was kept immersed in a mixture solution of ST (1.5mL) and EB (1.5 mL) for 1h, while in the intermediate time intervals 0.123 mL of the supernatant solution were pipetted out for recording the GC chromatogram at those respective times (Fig. S16).

For knowing the composition of the adsorbed MOF during the immersion test of ST/EB, the MOF samples subjected to these experiments viz., setups A, B and C were filtered out from the respective immersion solution(s), on completion of immersion-tenure i.e., 3hours. These were washed well with MeCN, and then digested in DCl, The DCl solutions were separately analyzed by GC by using the same method file (of GC) used for the supernatant solutions, effective to detect the presence of ST. No ligand peak was seen in the range of 2-40 minutes retention time using the specified scan parameters, mostly due to the highly polar nature of the constituent ligands, unlike to ST and EB.

GC Instrumentation: Materials and Methods:

GC-2014 Shimadzu Gas chromatograph (with AOC-20i Auto Injector) was used with the Column RTX-5 (Length: 30m, Inner diameter: 0.32 mm, Film thickness: 0.25 μm); Injection volume: 1 μL, Injection temperature: 200 °C, Initial Column temperature: 40 °C, Column heating range: 40-70 °C, heating at 1 °C/min. With this setup, we could obtain separate retention times for ST and EB. The results (Figures S14-S16) confirm that the observed decline in the signal intensity is solely in the presence of ST. The corresponding uptake times indicate convincingly fast kinetics of the process.

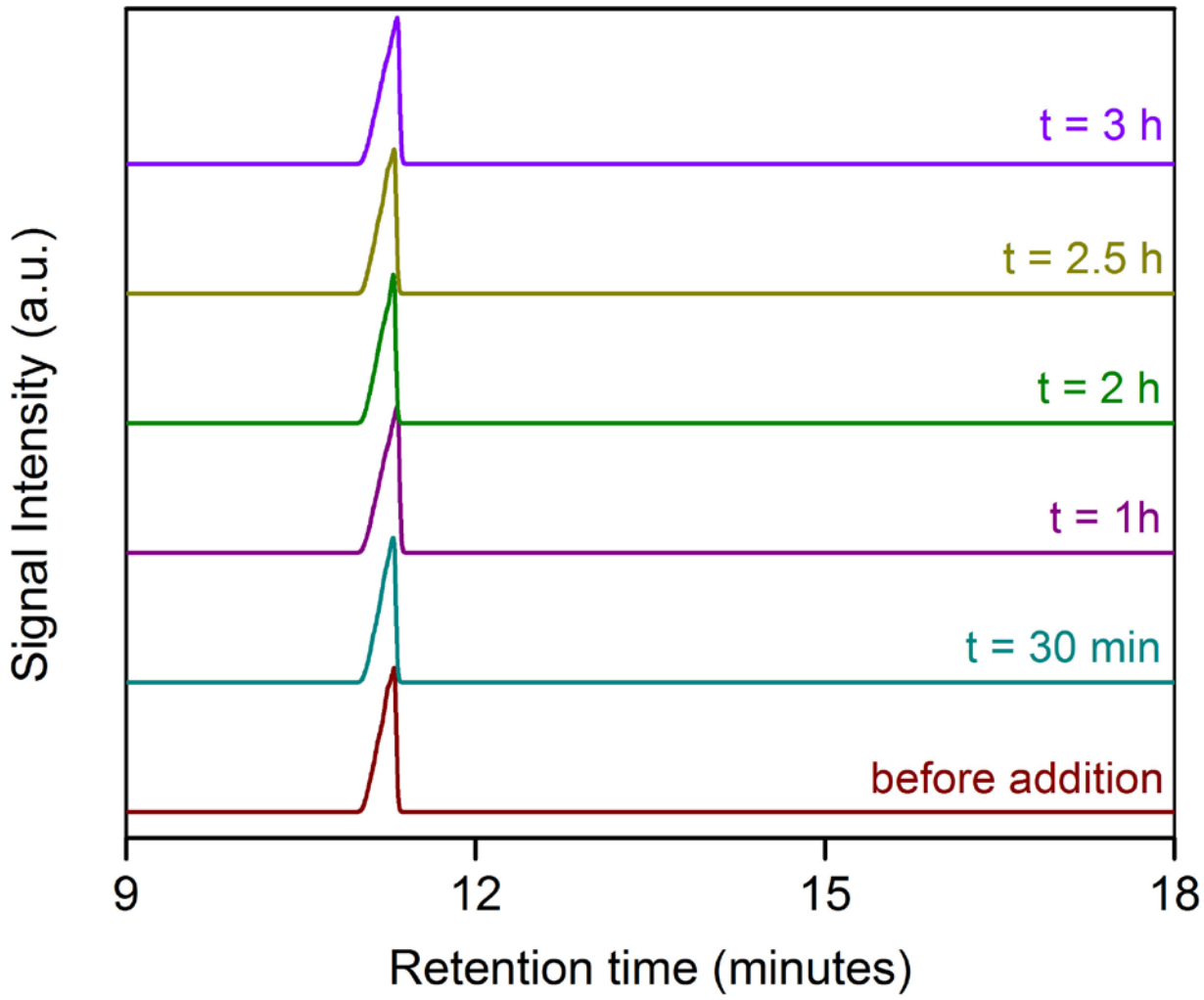

Figure S14. GC chromatogram of the supernatant solutions recorded at the specified time intervals in the setup A (ethyl benzene immersion test). Signals in each of the cases denote the contribution of EB only, intensity of which is remaining unchanged with increasing time of immersion with MOF.

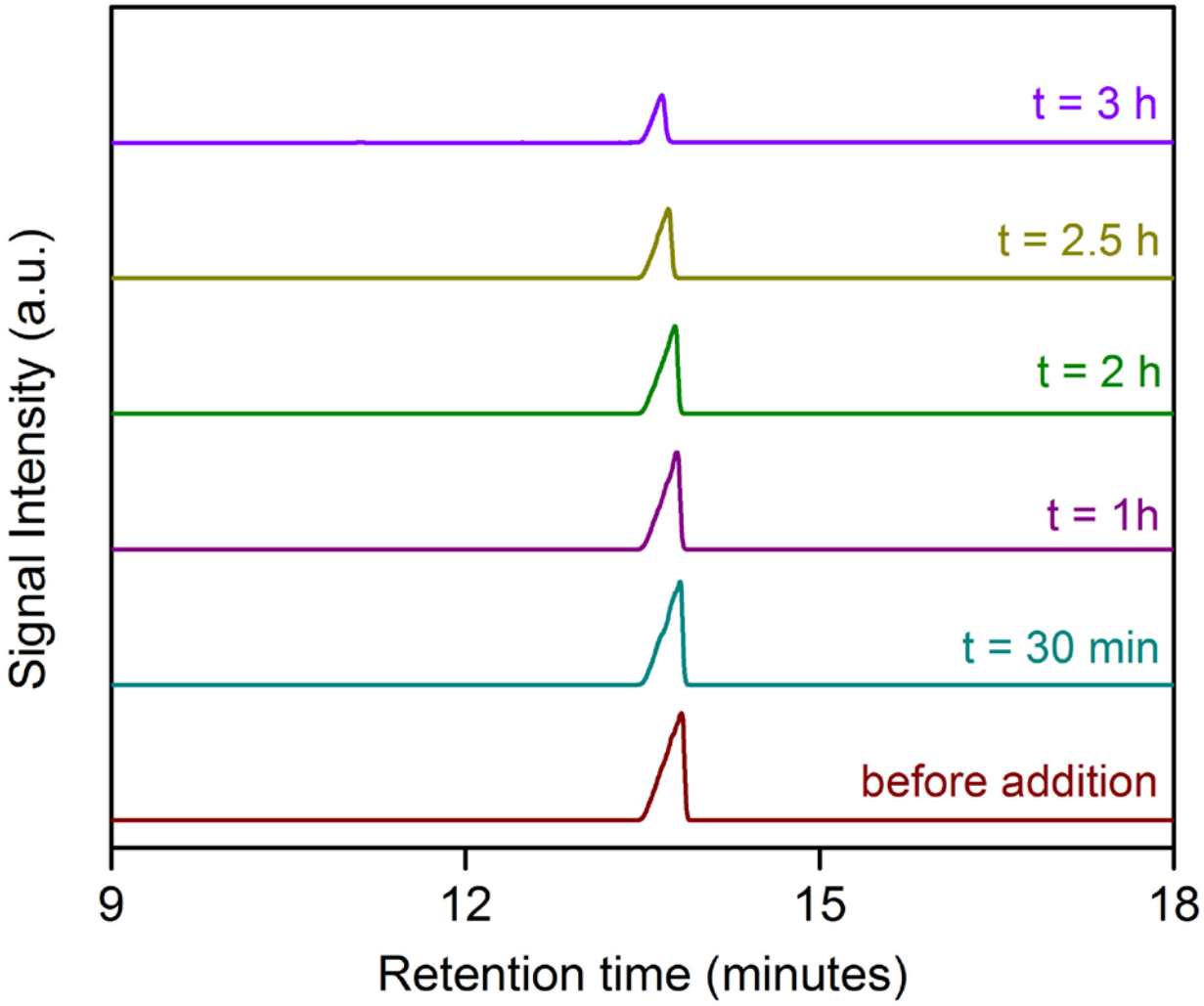

Figure S15. GC chromatogram of the supernatant solutions recorded at the specified time intervals in the setup B (styrene immersion test). Signals in each of the cases denote the contribution of ST only, intensity of which is getting steadily diminished with increasing time of immersion with MOF.

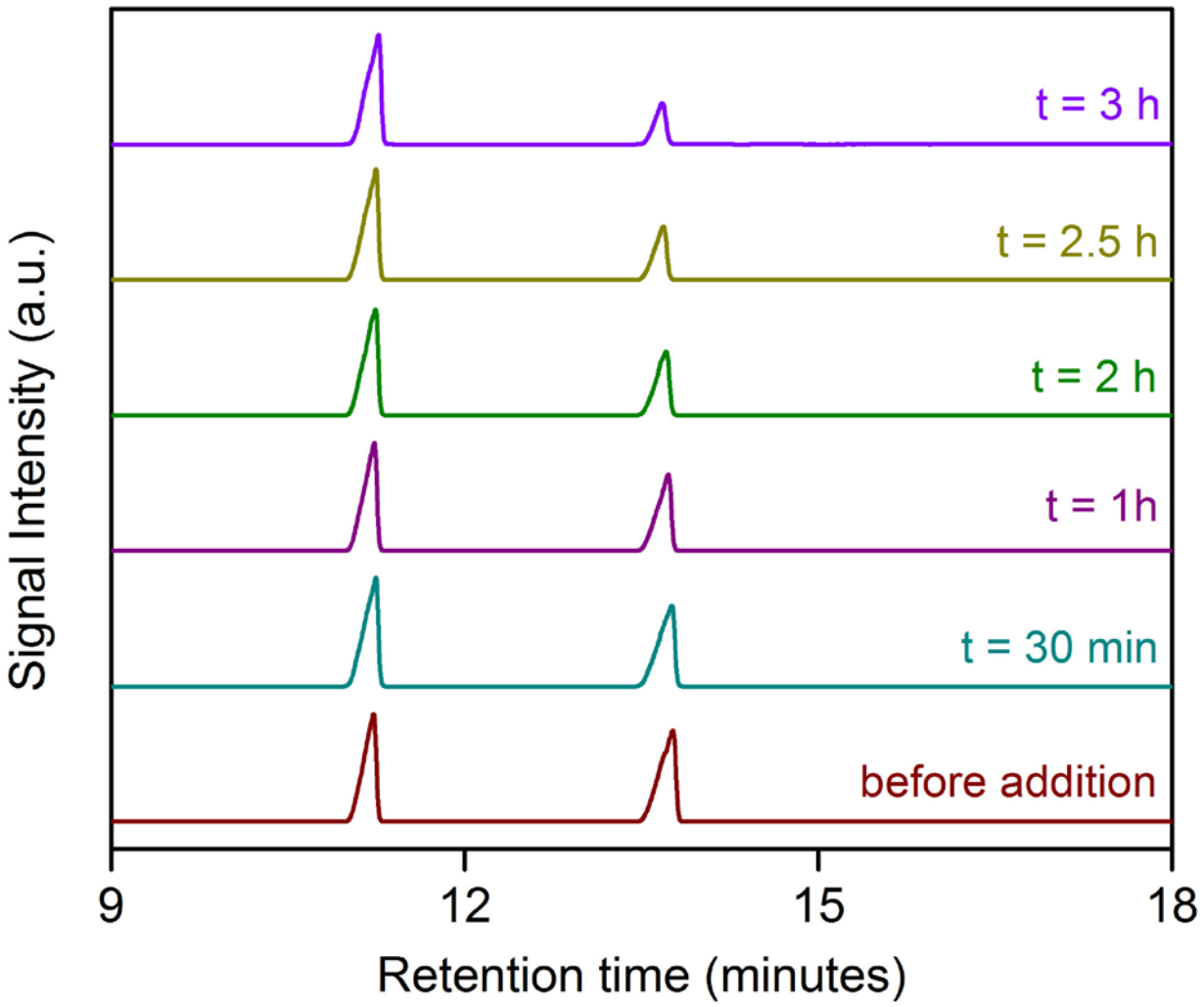

Figure S16. GC chromatogram of the supernatant solutions recorded at the specified time intervals in the setup C (ST/EB mixture immersion test). Signals in each of the cases denote the individual signal for the contribution of ST only, intensity of which is getting steadily diminished with increasing time of immersion with MOF.

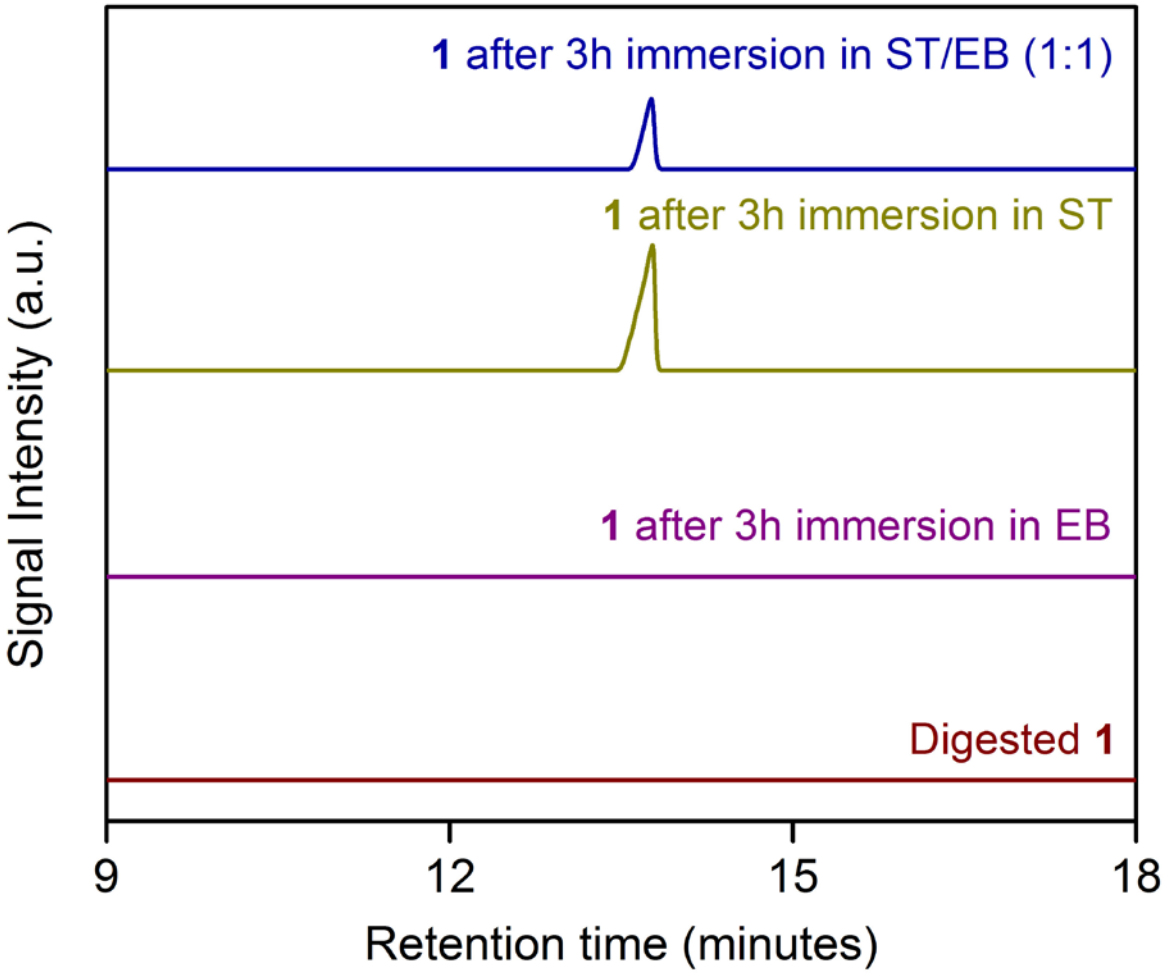

Figure S17. GC chromatogram of the DCl-digested DynaMOF-100, and all three different immersed MOF-phases after the completion of 3h immersion tenures in the GC experiment setups a, b and c as described above.

Recently Warren *et al.*[S1] reported a flexible MOF, Ce(HTPCB), synthesized by solvothermal reaction of $Ce(NO_3)_3.6H_2O$ with the tetradentate carboxylic acid H_4TCPB, which undergoes a framework reconstruction selectively to para-analogue among the different isomers of xylene. For *m*-xylene/*p*-xylene mixtures, Warren *et al.* has come up with adsorption selectivities in favor of *p*-xylene in the range of 4.6 – 6.[S1] This unprecedented finding provided much-needed insight into how flexible MOFs should be designed to maximize their selectivity for target molecules, as this report concluded that flexible structures those are initially mismatched in terms of fit and capacity to the preferred guest species, eventually turn out to be the potential candidates for efficient molecular separations.

Fitting of pure component isotherms in DynaMOF-100

The measured pure component isotherm data for each hydrocarbon exhibit hysteresis effects. For the purpose of analyzing the separation potential, we use on the "adsorption branch" of the isotherms and neglect the "desorption branch".

Some of the pure component isotherm data show marked inflections, and in order to correctly capture these inflections the unary isotherm data were fitted with the two-site Langmuir-Freundlich model:

$$q = q_{A,sat}\frac{b_A p^{\nu_A}}{1+b_A p^{\nu_A}} + q_{B,sat}\frac{b_B p^{\nu_B}}{1+b_B p^{\nu_B}} \quad (1)$$

The saturation capacities q_{sat}, Langmuir constants b, and the Freundlich exponents ν, are provided in Table S3. Figure S20a provides a comparison of the experimental isotherm data with the Langmuir-Freundlich fits.

IAST calculations of mixture adsorption equilibrium in DynaMOF-100

We use the Ideal Adsorbed Solution Theory (IAST) of Myers and Prausnitz[S2] to determine the adsorption equilibrium for equimolar gas phase 4-component equimolar *o*-xylene(1)/*m*-xylene(2)/*p*-xylene(3)/ethylbenzene(4) mixtures; see Figure S20b**.** We note that for pressures at 100 kPa, the adsorbed phase consists predominantly of *p*-xylene. In current industrial practice, the separation of xylene isomers is conducted with bulk liquid phase mixtures using BaX zeolite;

under such conditions the pores of BaX are saturated with guest molecules. For comparison with BaX and other MOFs, let us define the fractional occupancy within the pores, θ_t

$$\theta_t = \sum_{i=1}^{n} \frac{q_i}{q_{i,sat}} \tag{2}$$

where $q_{i,sat} = q_{i,A,sat} + q_{i,A,sat}$, is the sum of the saturation capacities of the two sites A and B in the dual-Langmuir-Freundlich isotherm fits.

Figure S20c shows the IAST calculations of the fractional occupancy, θ_t, within the pores of DynaMOF-100 as a function of the total gas phase pressure, p_t. We note that the pores are saturated, i.e. $\theta_t \rightarrow 1$, when the total pressure p_t has values exceeding about 4 kPa. Figure S20d shows the IAST calculations of the component loadings as a function of the fractional occupancy, θ_t, within the pores of DynaMOF-100. We note that at pore saturation conditions, i.e. $\theta_t \rightarrow 1$, the pore are predominantly occupied by *p*-xylene.

Let us now compare the adsorption selectivity and *p*-xylene uptake capacities of DynaMOF-100 with BaX and MAF-X8.

For a binary mixture the adsorption selectivity is defined as follows

$$S_{ads} = \frac{q_1/q_2}{p_1/p_2} \tag{3}$$

For separation of 4-component equimolar *o*-xylene(1)/*m*-xylene(2)/*p*-xylene(3)/ethylbenzene(4) mixtures we adopt the following definition of selectivity that was used in the recent paper of Torres-Knoop *et al.*[31]

$$S_{ads} = \frac{(q_3)/(q_1+q_2+q_4)}{(p_3)/(p_1+p_2+p_4)} = 3\frac{(q_3)}{(q_1+q_2+q_4)} \tag{4}$$

Figure S21a shows that the adsorption selectivity of DynaMOF-100 is about one to two orders of magnitude higher than that of MAF-X8 and BaX zeolite.

Besides adsorption selectivity, the separation performance is also dictated by the uptake capacity for *p*-xylene. Figure S21b compares the *p*-xylene uptake capacity of MAF-X8 (at 433 K), BaX zeolite (at 393 K, and 453 K), with that of DynaMOF-100 (at 298 K). We note that at pore saturation conditions, that is typical of industrial operations, DynaMOF-100 has a significantly higher uptake capacity than BaX and MAF-X8.

Transient breakthrough simulations

The separation performance of a fixed bed adsorber (see schematic in Figure S22); is dictated by both adsorption selectivity and capacity. A higher capacity to adsorb *p*-xylene leads to a longer cycle time that is desirable because of this requires less frequent regeneration.

Using the pure component isotherm fits of experimental data, we carried out transient breakthrough simulations using the methodology described in detail in our earlier works.[S3–S4]

The breakthrough characteristics for any component is essentially dictated primarily by the characteristic contact time $\frac{L}{v}=\frac{L\varepsilon}{u}$ between the crystallites and the surrounding fluid phase. It is common to use the dimensionless time, $\tau=\frac{tu}{L\varepsilon}$, obtained by dividing the actual time, *t*, by the characteristic time, $\frac{L\varepsilon}{u}$ when plotting simulated breakthrough curves.[S4] For the breakthrough simulations reported here we use the parameter values: L = 0.3 m; voidage of bed, ε = 0.4; interstitial gas velocity, v = 0.1 m/s; superficial gas velocity, u = 0.04 m/s.

The clearest demonstration of the propensity of DynaMOF-100 to selectively adsorb *p*-xylene is provided by pulse chromatographic simulations; see Figure S23a. The elution sequence of the pulses is ethylbenzene, *m*-xylene, *o*-xylene, and *p*-xylene. The mean times at which the pulses appear are τ = 30 (ethylbenzene, and *m*-xylene), τ = 300 (o-xylene), and τ = 10000 (*p*-xylene). The largest time lag between the elution of *o*-xylene and *p*-xylene is a clear indication of the efficacy of separation.

Let us now consider transient breakthroughs with step-input of four-component mixture of C8 hydrocarbons. Figure S23b shows the results of transient breakthrough simulations of a 4-component equimolar *o*-xylene(1)/*m*-xylene(2)/*p*-xylene(3)/ethylbenzene(4) mixtures with step input: p_i = 1 kPa for each hydrocarbon; this choice of partial pressures ensures that the conditions correspond to pore saturation (*cf.* Figure S20c). *o*-xylene, *m*-xylene and ethylbenzene are hardly adsorbed and are rejected into the bulk fluid phase immediately after feed injection.

For comparison with other MOFs, we define the cycle time for *p*-xylene as the dimensionless time, τ_{cycle}, at which the concentration of the gas at the outlet is 99% of the value at the inlet; this approach was used earlier in the comparisons published by Torres-Knoop *et al.*[31] in Figure 6b of their paper. The cycle time τ_{cycle} = 10186 for DynaMOF-100, as compared to τ_{cycle} = 335 for

MAF-X8, and τ_{cycle} = 74 for BaX zeolite. Longer cycle times are desirable because this implies that implies that smaller desorbent-flow rates will be required.

The clean separation achieved with DynaMOF-100 is best illustrated by video animations of the breakthroughs using both step input and pulse input of *o*-xylene/*m*-xylene/*p*-xylene/ethylbenzene mixtures.

Conclusions

DynaMOF-100 is the best material for selective adsorption of *p*-xylene from a mixture of C8 hydrocarbons. The separations with DynaMOF-100 are significantly better than that of BaX zeolite, which is currently in use for industrial applications, and also MAF-X8.

Ethylbenzene/Styrene Separations with MIL-47(V) and MIL53(Al)

The pure component isotherm data, measured for, of Maes *et al.*[28] (*cf.* Figures S18a, and S18b) show the adsorption loadings of styrene are higher than that of ethylbenzene. Figures S19a, and S19b compare the experimental data for transient breakthroughs of ethylbenzene/styrene mixtures in MIL-47(V) and MIL-53(Al) with corresponding breakthrough simulations using the methodology described in our earlier work.[S3] Two types of simulations were performed: (a) assuming thermodynamic equilibrium, and (b) with inclusion of intra-crystalline diffusion. The sequence of breakthroughs is unaltered due to inclusion of diffusion limitations. Diffusional limitations lead to distended, *i.e.* non-sharp, breakthroughs, in agreement with the liquid phase experimental breakthrough data of Maes *et al.*[28] The agreement between experimental breakthroughs and our breakthrough simulations lends credibility to the applicability of the Ideal Absorbed Solution Theory (IAST) calculations.

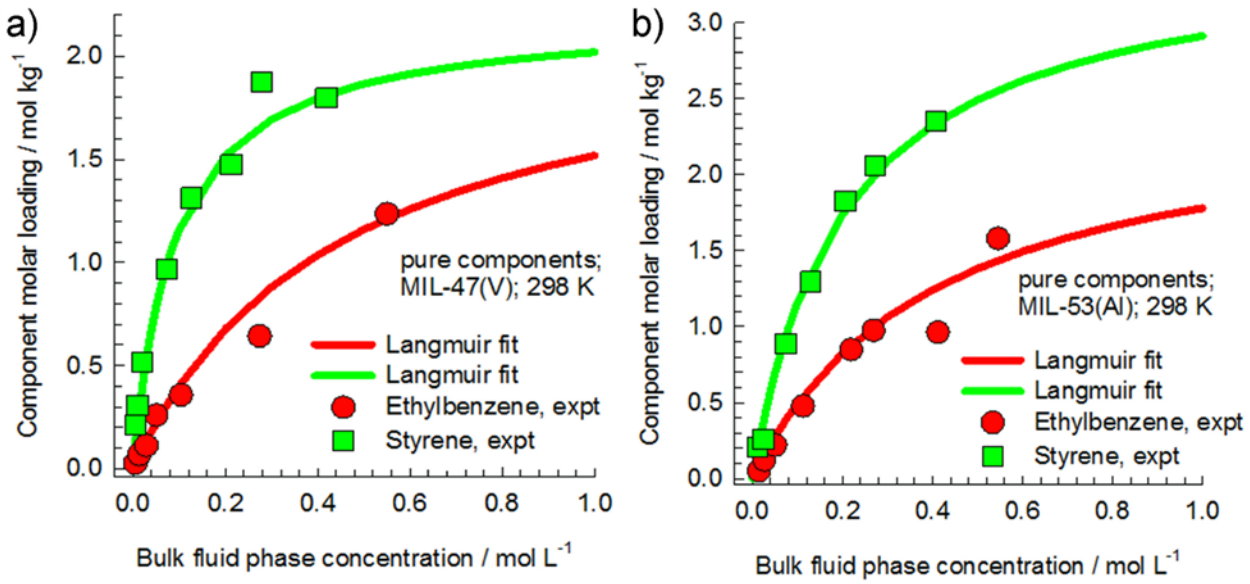

Figure S18. Comparison of experimental data for pure component isotherms for ethylbenzene and styrene in MIL-47(V) and MIL-53(Al) with Langmuir fits that are shown by the continuous solid lines. The isotherms used in the simulations are the experimental data reported by Maes *et al.*;[28] the Langmuir fit parameters are specified in tables S1 and S2.

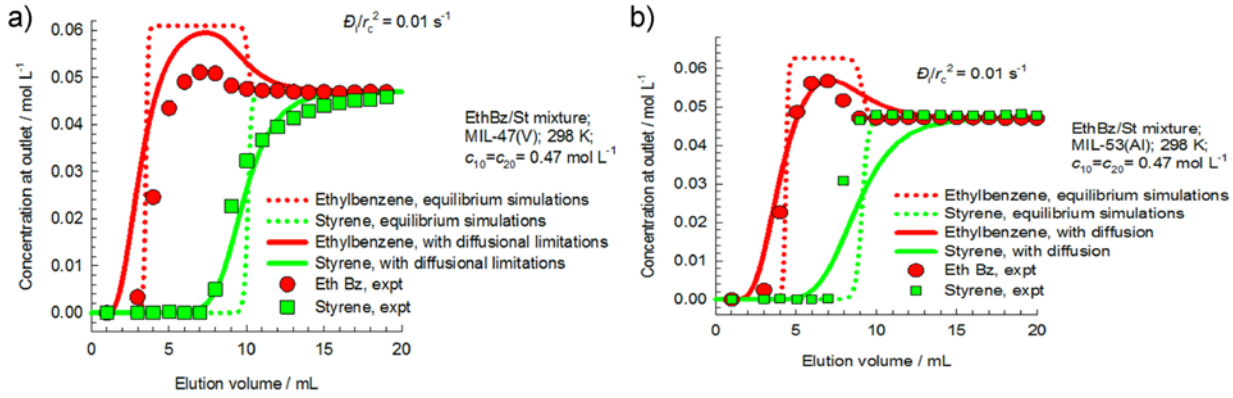

Figure S19. (a, b) Breakthrough simulations for ethylbenzene/styrene mixtures in (a) MIL-47(V), and (b) MIL-53(Al) at 298 K. The operations are in the liquid phase, with step inputs of feed concentrations c_{i0} = 0.47 mol L-1 in both cases. The dotted lines are simulations assuming thermodynamic equilibrium. The continuous solid lines represent breakthrough simulations with inclusion of intra-crystalline diffusion, neglecting thermodynamic coupling. The large symbols are the experimental breakthrough data, scanned from figures 2a and 2b of the paper by Maes *et al.*[28] The isotherms used in the simulations are the experimental data reported by Maes *et al.*; [28] the Langmuir fit parameters are specified in tables S1 and S2.

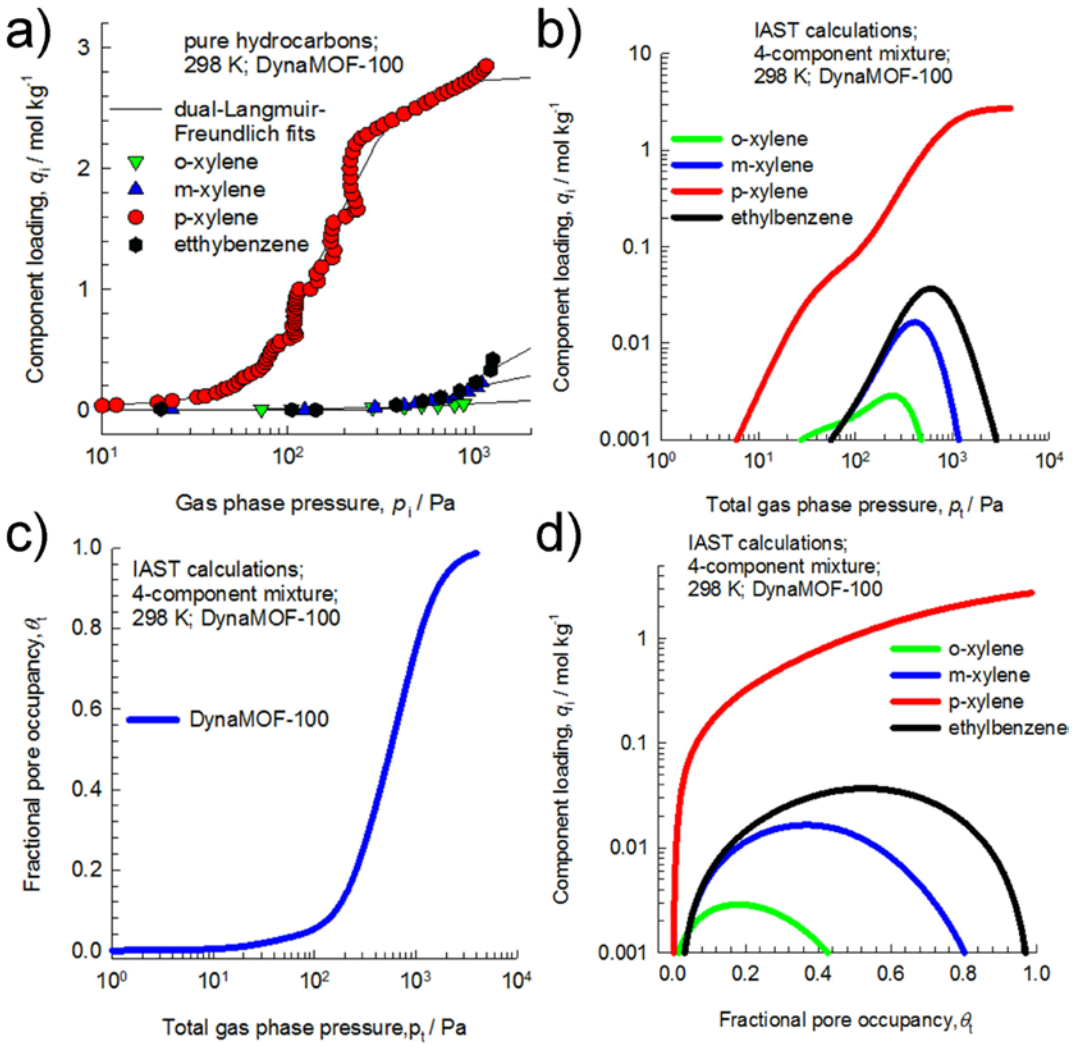

Figure S20. a) Comparison of experimental data for pure component isotherms in DynaMOF-100 with Langmuir-Freundlich fits (parameters specified in Table 1), that are shown by the continuous solid lines; b) Calculations using the Ideal Adsorbed Solution Theory (IAST) of Myers and Prausnitz[S2] to determine the adsorption equilibrium for equimolar gas phase 4-component *o*-xylene/*m*-xylene/*p*-xylene/ethylbenzene mixtures in DynaMOF-100 at 298 K. The *x*-axis is the total gas phase pressure; c) IAST calculations of the fractional occupancy, θ_t, within the pores of DynaMOF-100 as a function of the total gas phase pressure, p_t. The calculations are for equimolar gas phase 4-component *o*-xylene/*m*-xylene/*p*-xylene/ethylbenzene mixtures in DynaMOF-100 at 298 K; d) IAST calculations of the component loadings in equilibrium with equimolar gas phase 4-component *o*-xylene/*m*-xylene/*p*-xylene/ethylbenzene mixtures in DynaMOF-100 at 298 K. The *x*-axis is fractional occupancy, θ_t, within the pores of DynaMOF-100.

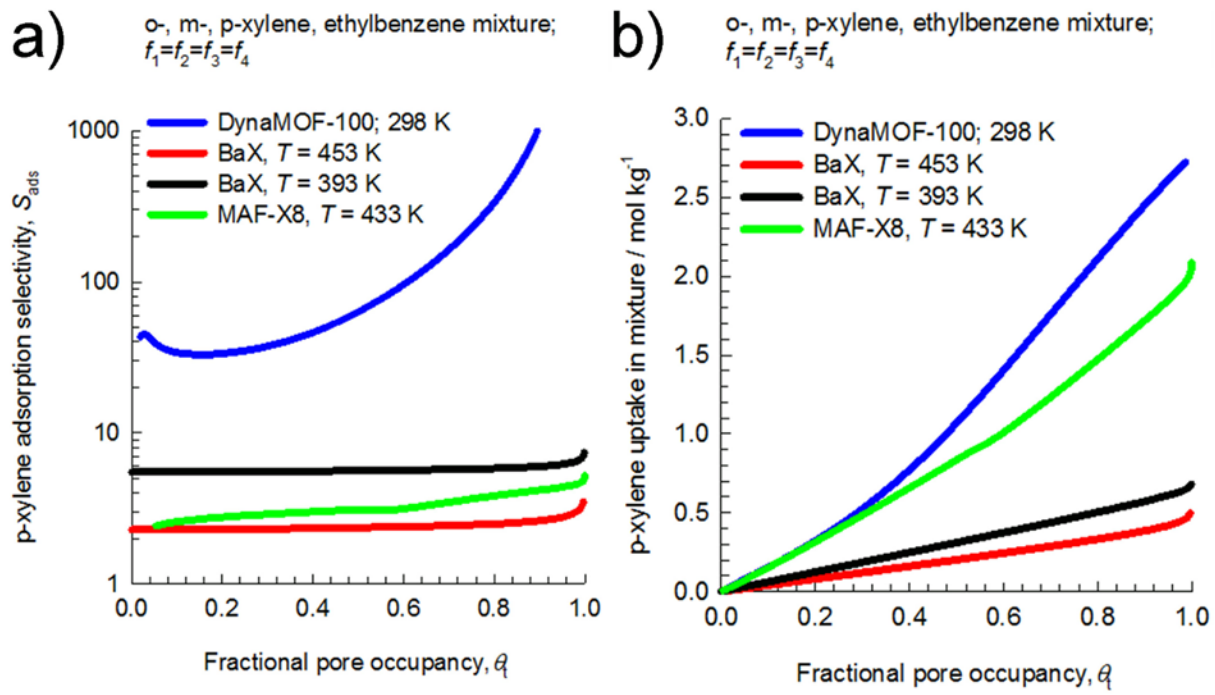

Figure S21. a) IAST calculations for *p*-xylene adsorption selectivity for 4-component *o*-xylene(1)/*m*-xylene(2)/*p*-xylene(3)/ethylbenzene(4) mixture in MAF-X8 (at 433 K), BaX zeolite (at 393 K, and 453 K), and DynaMOF-100 (at 298 K). The *x*-axis is fractional occupancy, θ_t, within the pores of the MOFs; b) IAST calculations for *p*-xylene uptake capacity for 4-component *o*-xylene(1)/*m*-xylene(2)/*p*-xylene(3)/ethylbenzene(4) mixture in MAF-X8 (at 433 K), BaX zeolite (at 393 K, and 453 K), and DynaMOF-100 (at 298 K). The *x*-axis is fractional occupancy, θ_t, within the pores of the MOFs.

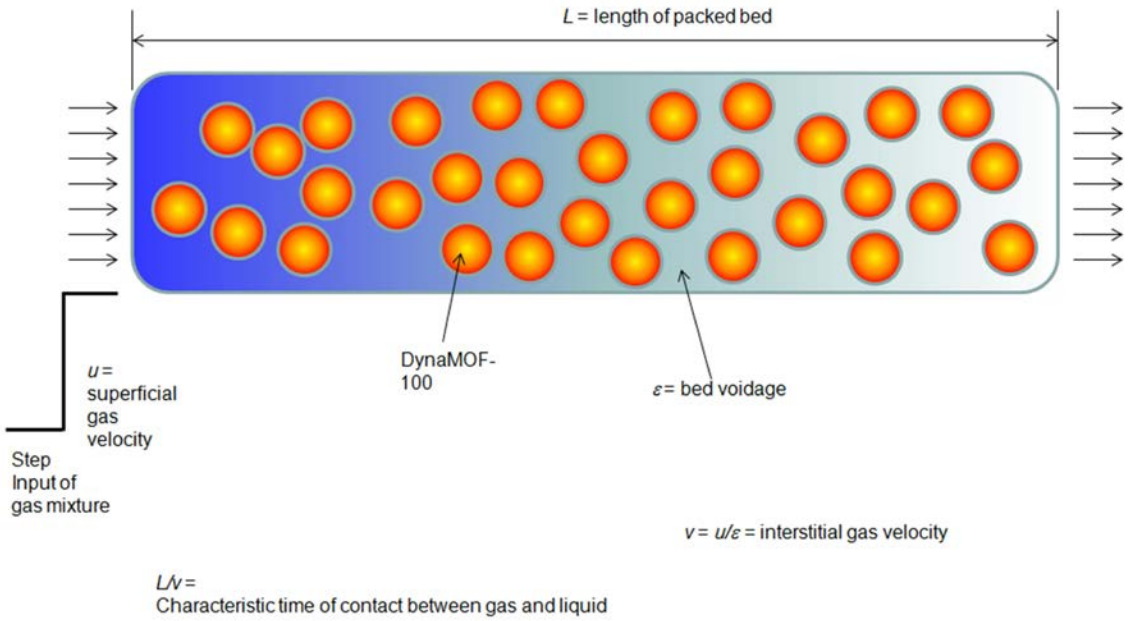

Figure S22. Schematic of a packed bed adsorber.

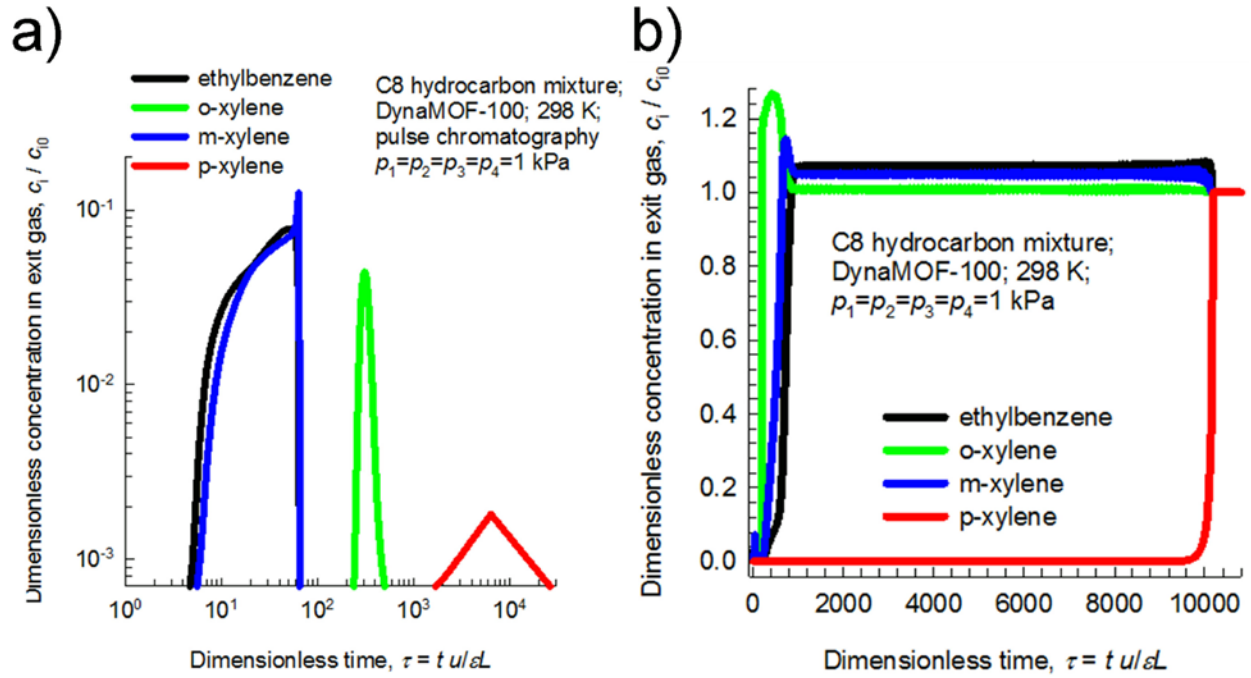

Figure S23. a) Pulse chromatographic simulations of the breakthrough of 4-component *o*-xylene(1)/*m*-xylene(2)/*p*-xylene(3)/ethylbenzene(4) mixture in packed bed of DynaMOF-100 at 298 K. The inlet gas phase has partial pressures of 1 kPa for each component. The duration of the pulse is 10 s; b) Transient breakthrough simulations for 4-component *o*-xylene(1)/*m*-xylene(2)/*p*-xylene(3)/ethylbenzene(4) mixture in packed bed of DynaMOF-100 at 298 K. The inlet gas phase has partial pressures of 1 kPa for each component.

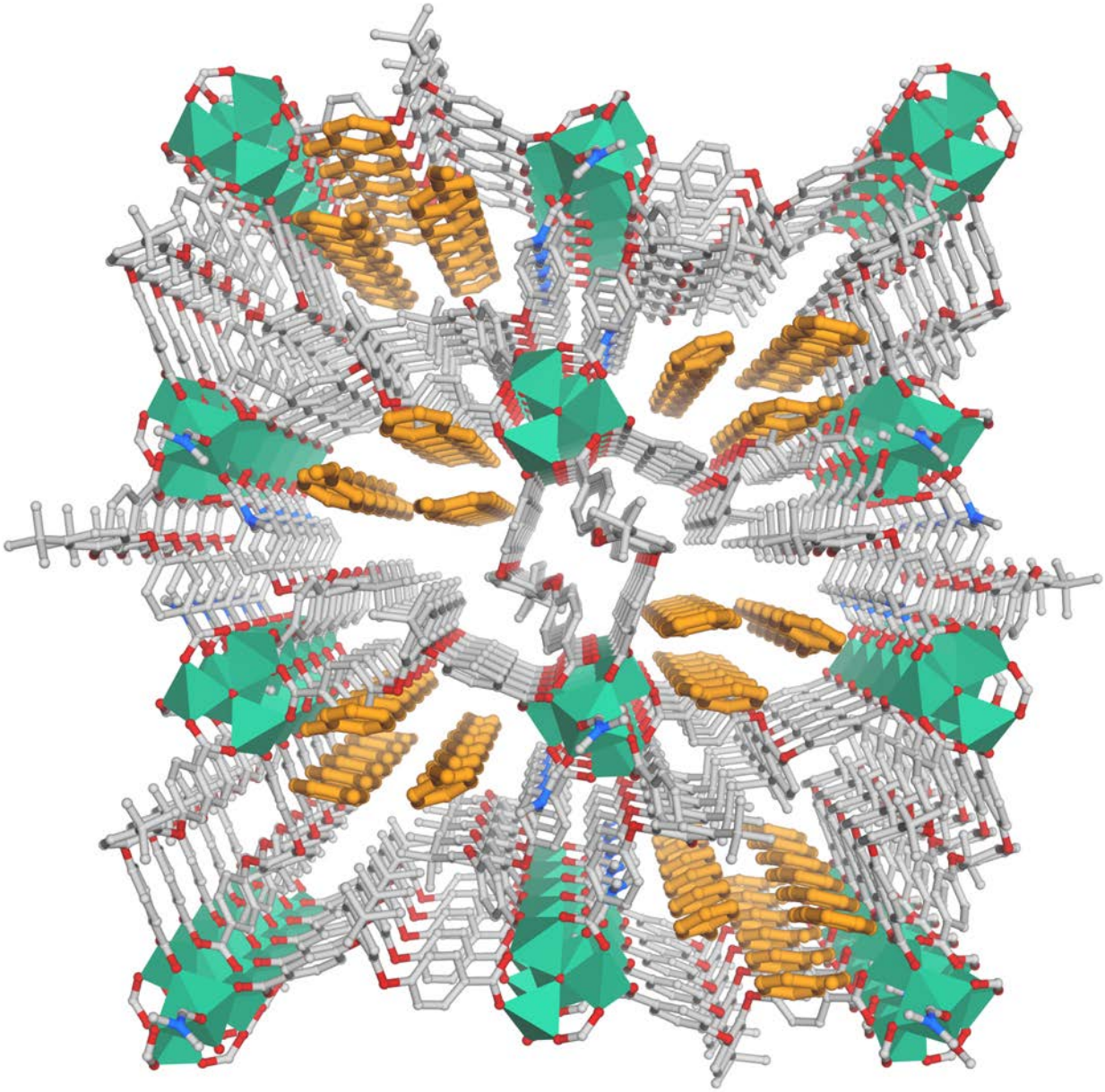

Figure S24. Resolvated framework on styrene accommodation-mediated breathing phenomenon.

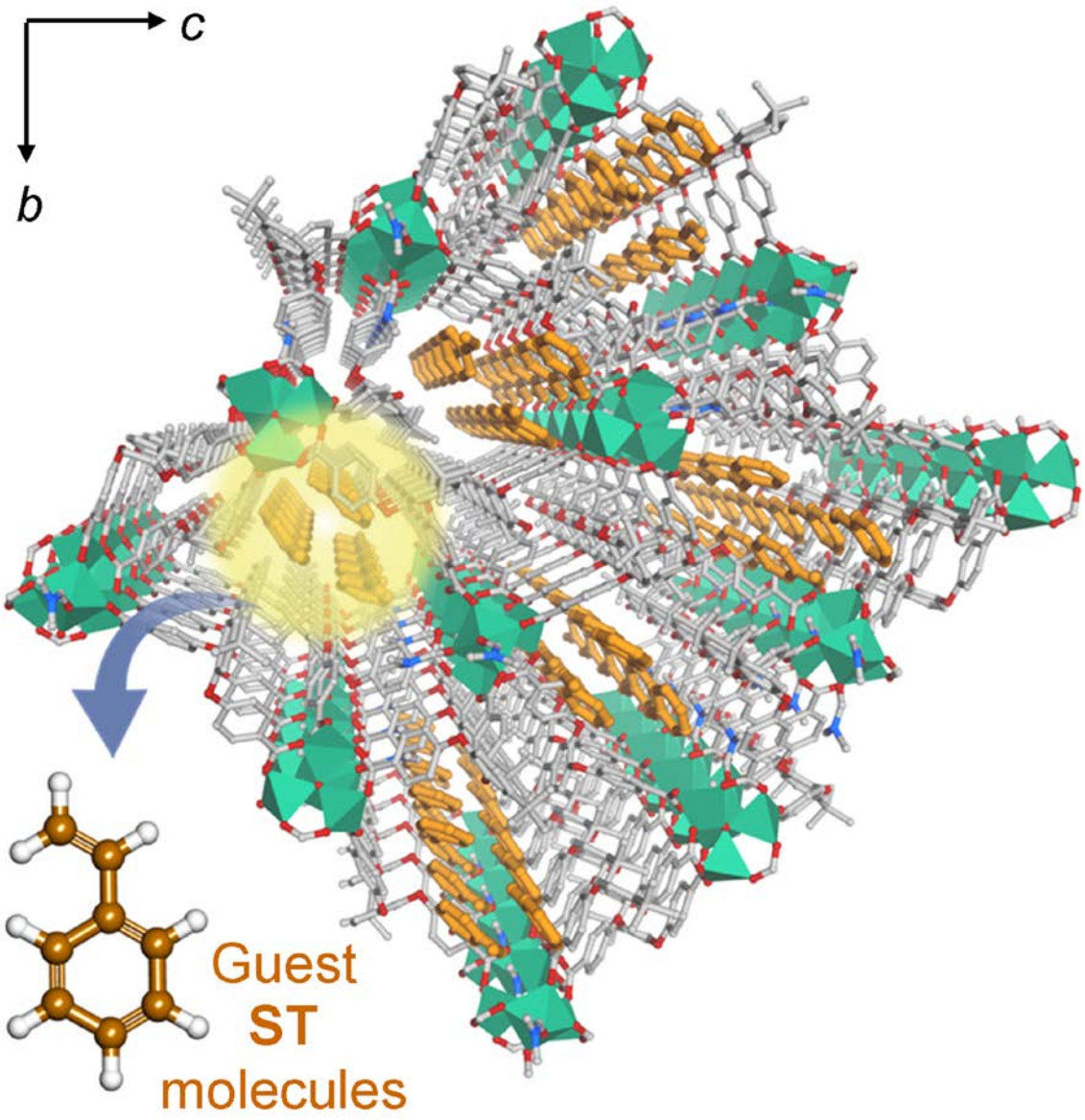

Figure S25. Perspective view of the Resolvated framework, viewed along crystallographic *a*-axis.

Table S1. Langmuir-Freundlich parameters for ethylbenzene and styrene at 298 K in MIL-47(V). The experimental data are scanned for Figure S1 of Maes *et al.*[28]

$$q = q_{sat}\frac{bc}{1+bc}$$

	q_{sat} mol kg^{-1}	b $\left[\text{mol L}^{-1}\right]^{-1}$
ethylbenzene	2.2	2.23
Styrene	2.2	11.15

Table S2. Langmuir-Freundlich parameters for ethylbenzene and styrene at 298 K in MIL-53(Al). The experimental data are scanned for Figure S2 of Maes *et al.*[28]

$$q = q_{sat}\frac{bc}{1+bc}$$

	q_{sat} mol kg^{-1}	b $\left[\text{mol L}^{-1}\right]^{-1}$
ethylbenzene	2.5	2.48
Styrene	3.5	4.96

Table S3. Dual-site Langmuir-Freundlich parameters for aromatic hydrocarbons at 298 K in DynaMOF-100.

	Site A			Site B		
	$q_{i,A,sat}$ mol kg^{-1}	$b_{i,A}$ Pa$^{-\nu_{iA}}$	$\nu_{i,A}$ dimensionless	$q_{i,B,sat}$ mol kg^{-1}	$b_{i,B}$ Pa$^{-\nu_{iA}}$	$\nu_{i,B}$ dimensionless
o-xylene (OX)	0.15	5.57×10^{-4}	1			
m-xylene (MX)	0.3	5.27×10^{-11}	3.5			
p-xylene (PX)	0.06	5.98×10^{-3}	2.3	2.7	4.56×10^{-6}	2.4
Ethylbenzene (EB)	0.56	6.57×10^{-12}	3.7			
Benzene (BZ)	0.3	1.7×10^{-2}	0.86	2.5	6.58×10^{-8}	2.3
Toluene (TL)	1.2	3.26×10^{-3}	0.92	2.1	5.7×10^{-10}	3.5
Cyclohexane (CY)	0.8	4.04×10^{-4}	0.76	2.5	1.06×10^{-22}	6.4
Styrene (ST)	3.9	4.29×10^{-09}	3.7			

The calculated molar volume (MVL)and minimum dimensions (MIN-1 and MIN-2) for styrene were calculated in a fashion similar to that described previously,[S5-S6] except that the three-dimensional points derived from the GEPOL algorithm[S7-S8] were calculated by Gaussian 09[S9] instead of ZINDO.[S10] For simple organic molecules, INDO/1 optimized geometries were used for single-point calculations with Gaussian 09. Verbose debug output [IOP(3/33=9)] from the Gaussian 09 implementation of GEPOL was used with the SCRF keyword [SCRF(G03Defaults,PCM,Read)] and the No Symmetry keyword to obtain the required output (using the second set of data for the molecular volumes and MIN's). As in the original paper, the Bondi radii[S11] (RADII=BONDI) and the van der Waals surface (Surface=VDW) were used; and the calculated MIN values do not include the reaction field correction factor (Alpha=1.0). The MVL was derived from the correlation reported in the original paper.[S5] For styrene, the calculated mVG ($Å^3$ $molecule^{-1}$), *M*VG (mL $mole^{-1}$), and the MVL (mL $mole^{-1}$) are 112.121, 67.519, and 116.997, respectively. The experimental molar volume, MV_{EXP} ($mL\,mol^{-1}$), for styrene is 114.577.

Table S4 Dimensions of Adsorptive molecules (Å)[S5]
(each atom surrounded by a van der Waals sphere)

	x	***y***	**z**	**MIN-1**	**MIN-2**
ST	9.721	3.331	6.784	3.331	6.784
EB	6.625	5.285	9.361	5.285	6.625
PX	6.618	3.81	9.146	3.81	6.618
MX	8.994	3.949	7.315	3.949	7.258
OX	7.269	3.834	7.826	3.834	7.269

MIN-1: Size of the adsorptive in the minimum dimension.

MIN-2: Second minimum dimension for molecular orientations that enable a molecule to enter the channel.

Table S5. Crystal data and structure refinement for Compound **1⊃ST'**.

Identification code	Compound **1⊃ST'**	
Empirical formula	C_{102} H_{74} N_2 O_{21} Zn_4	
Formula weight	1925.11	
Temperature	100(2) K	
Wavelength	0.71073 Å	
Crystal system	Monoclinic	
Space group	*P 21/c*	
Unit cell dimensions	*a* = 11.9745(10) Å	α= 90°.
	b = 32.827(3) Å	β= 98.614(2)°.
	c = 25.847(2) Å	γ = 90°.
Volume	10,045.6(15) $Å^3$	
Z	4	
Density (calculated)	1.273 Mg/m^3	
Absorption coefficient	1.011 mm^{-1}	
F(000)	3952	
Crystal size	0.16 x 0.14 x 0.12 mm^3	
Theta range for data collection	1.010 to 28.080°.	
Index ranges	-15<=h<=15, -41<=k<=43, -34<=l<=34	
Reflections collected	181405	
Independent reflections	24239 [R(int) = 0.0878]	
Completeness to theta = 25.242°	100.0 %	
Refinement method	Full-matrix least-squares on F^2	
Data / restraints / parameters	24239 / 135 / 1049	
Goodness-of-fit on F^2	1.061	
Final R indices [I>2sigma(I)]	R_1 = 0.1094, wR_2 = 0.3114	
R indices (all data)	R_1 = 0.1701, wR_2 = 0.3426	
Largest diff. peak and hole	1.497 and -0.652 e.$Å^{-3}$	

Notation

b_A	dual-Langmuir-Freundlich constant for species *i* at adsorption site A, $Pa^{-\nu_i}$
b_B	dual-Langmuir-Freundlich constant for species *i* at adsorption site B, $Pa^{-\nu_i}$
c_i	molar concentration of species *i* in fluid mixture, mol m^{-3}
c_{i0}	molar concentration of species *i* in fluid mixture at inlet to adsorber, mol m^{-3}
L	length of packed bed adsorber, m
n	number of species in the mixture, dimensionless
p_i	partial pressure of species *i* in mixture, Pa
p_t	total system pressure, Pa
q_i	component molar loading of species *i*, mol kg^{-1}
$q_{i,sat}$	molar loading of species *i* at saturation, mol kg^{-1}
q_t	total molar loading in mixture, mol kg^{-1}
$q_{sat,A}$	saturation loading of site A, mol kg^{-1}
$q_{sat,B}$	saturation loading of site B, mol kg^{-1}
t	time, s
T	absolute temperature, K
u	superficial gas velocity in packed bed, m s^{-1}
v	interstitial gas velocity in packed bed, m s^{-1}

Greek letters

ε	voidage of packed bed, dimensionless
ν	exponent in dual-Langmuir-Freundlich isotherm, dimensionless
θ_t	fractional occupancy within the pores, dimensionless
ρ	framework density, kg m^{-3}
τ	time, dimensionless

Subscripts

i	referring to component *i*
A	referring to site A
B	referring to site B
t	referring to total mixture

References:

S1. Warren, J. E.; Perkins, C. G.; Jelfs, K. E.; Boldrin, P.; Chater, P. A.; Miller, G. J.; Manning, T. D.; Briggs, M. E.; Stylianou, K. C.; Claridge, J. B.; Rosseinsky, M. J. *Angew. Chem. Int. Ed.* **2014**, *53*, 4592-4596.

S2. Myers, A. L.; Prausnitz, J. M. *A.I.Ch.E.J.* **1965**, *11*, 121-130.

S3. Krishna, R. *Microporous Mesoporous Mater.* **2014**, *185*, 30-50.

S4. Krishna, R.; Long, J. R. *J. Phys. Chem. C* **2011**, *115*, 12941-12950.

S5. Webster, C. E.; Drago, R. S.; Zerner, M. C. *J. Am. Chem. Soc.***1998**, *120*, 5509-5516.

S6. Webster, C. E.; Drago, R. S.; Zerner, M. C. *J. Phys. Chem. B* **1999**, *103*, 1242-1249.

S7. Pascual-Ahuir, J. L.; Silla, E.; Tunon, I. In *GEPOL93*.; Silla, E.; Tunon, I.; Pascual Ahuir, J. L. *J. Comput. Chem.* **1994**, *15*, 1127-1138.

S8. Silla, E.; Tunon, I.; Pascual-Ahuir, J. L. *J. Comput. Chem.* **1991**, *12*, 1077-1088.

S9. Frisch, M. J. *et al. Gaussian 09*; Revision D.01 ed.; Gaussian, Inc.: Wallingford CT, **2009**.

S10. Zerner, M. C.; Ridley, J. E.; Bcon, A. D.; Edwards, W. D.; Head, J. D.; McKelvey, J.; Culberson, J. C.; Knappe, P.; Cory, M. G.; Weiner, B.; Baker, J. D.; Parkinson, W. A.; Kannis, D.; Yu, J. ; Rösch, N.; Kotzian, M.; Tamm, T.; Karelson, M. M.; Zheng, X.; Pearl, G. M.; Broo, A.; Albert, K.; Cullen, J. M.; Cramer, C. J.; Truhlar, D. G.; Li, J.; Hawkins, G. D.; Liotard, D. A. ZINDO, a semiempirical program package, University of Florida, Gainesville, FL.

S11. Bondi, A. *J. Phys. Chem.* **1964**, *68*, 441-451.